Fronto-motor circuits linked to effort-based decision-making and apathy in healthy subjects

Gerard Derosiere[1,2,*], Pierre Vassiliadis[3], Laurence Dricot[1], Quentin Dessain[1], Nicolas Delinte[1], Alexandre Zénon[4], Julie Duque[1]

[1] Institute of Neuroscience, Université Catholique de Louvain, 1200, Brussels, Belgium.

[2] Université Claude Bernard Lyon 1, CNRS, INSERM, Centre de Recherche en Neurosciences de Lyon (CRNL), U1028 UMR5292, Impact Team, F-69500, Bron, France.

[3] Defitech Chair of Clinical Neuroengineering, Neuro-X Institute, École Polytechnique Fédérale de Lausanne (EPFL), Geneva and Sion, Switzerland.

[4] INCIA, CNRS, Bordeaux, France

* Contact information:

Email address: gerard.derosiere@inserm.fr

Twitter: @GDerosiere

SUMMARY

Apathy is a syndrome characterized by a disruption in effort-reward decision-making, accompanied by structural and functional changes in a related fronto-basal ganglia (BG) network. While activity changes in the primary motor cortex (M1) during effort and reward valuation have been repeatedly observed, previous work on apathy has largely overlooked the connections between the fronto-BG network and M1, potentially missing key circuits in the apathy network. This study addresses this gap by investigating structural and effective connectivity in fronto-M1, fronto-BG-M1, and intra-M1 circuits in relation to apathy in 45 healthy subjects. Behavior was assessed using a battery of apathy-related questionnaires and computational modeling of effort and reward valuation in a decision-making task. Fronto-motor circuits were examined through a combination of MRI-derived tractography and paired-pulse transcranial magnetic stimulation, which probed structural and effective connectivity, respectively. The data reveal that apathy scores are associated with both structural and effective connectivity in fronto-M1 and fronto-BG-M1 circuits. Circuits originating from the supplementary motor area primarily index effort valuation, while connectivity in intra-M1 GABAergic circuits correlates exclusively with reward valuation. These findings suggest that distinct fronto-motor circuits are linked to different dimensions of motivated behavior and may constitute specific neuromodulation targets for patients suffering from apathy.

KEYWORDS

Effort valuation, reward valuation, cost-benefit decision-making, motor cortex, motivation

INTRODUCTION

Apathy, a syndrome marked by a diminished willingness to exert efforts for rewards[1–11], is highly prevalent in many brain disorders. It is found in 47% of schizophrenia cases, 61% of traumatic brain injury cases, 40% of Parkinson's Disease cases and up to 72% of frontotemporal dementia cases[12,13]. This prevalence highlights the need for research into the neural bases of apathy, to understand its biology, develop biomarkers, and identify circuits for targeted treatments[10,14]. Notably, studies of apathy in clinical populations can be confounded by neural changes associated with compensatory mechanisms or the pathology itself and often rely on small patient cohorts classified as either apathetic or non-apathetic, limiting their power[15]. A promising approach to identify the brain circuits underlying apathy is to study continuous apathy levels in larger groups of healthy individuals[16–18]. Interestingly, apathy levels vary significantly even among healthy individuals, with some showing high apathy scores[17–21]. Despite this, the neurobiology of apathy levels in the general population remains largely unexplored.

It has become clear that apathy is not linked to a single brain region but can rather be seen as a network disorder[13,18,22–26]. Apathy is tied to increases and decreases in the volume and activity of distributed fronto-basal ganglia (BG) structures known for their role in deciding to exert efforts for rewards[13,22,23]. These structures include the supplementary motor area (SMA)[18], involved in effort valuation[27,28], the orbitofrontal cortex (OFC)[29], engaged in reward valuation[30,31], and the nucleus accumbens[32,33], thought to weigh up efforts and rewards[22,34]. Beyond these grey matter changes, recent studies show that apathy may also be linked to increases or decreases in white matter connectivity between some of these fronto-BG structures[18,24–26]. Such findings begin to outline what may constitute the apathy "dysfunctome"[35] – *i.e.*, the set of connections altered in apathy that may be tuned by targeted treatments. Strikingly though, while theories of decision-making increasingly recognize the crucial role of the primary motor cortex (M1) and its interactions with other brain regions[36–38], previous work on apathy has largely overlooked the brain's output structures, potentially missing key circuits in the apathy network. Yet, activity changes related to effort and reward valuation during decision-making have been observed repeatedly in M1 in rodents[39,40], non-human primates[41] and humans[42–46], suggesting a potential functional

link between the fronto-BG structures mentioned above and M1 that may be central to effort-based decisions[47] and, presumably, to apathy.

In the past two decades, progress in neuroimaging and brain stimulation have enabled new ways to explore this idea in humans. Advanced analyses of diffusion-weighted imaging (DWI) such as streamline tractography allow quantifying how structural connectivity in specific circuits varies among individuals[48,49]. Additionally, paired-pulse transcranial magnetic stimulation (ppTMS) allows pre-activating certain circuits and measuring the impact of this pre-activation on neural activity in M1's corticospinal neurons[38,50,51], providing a measure of how effective connectivity in circuits projecting to these neurons varies among individuals. Integrating these complementary methods through a multimodal framework thus provides a unique opportunity to investigate the different circuits connecting SMA, OFC and the BG to M1 in a comprehensive way.

In this study, we leveraged such a multimodal framework to examine structural and effective connectivity within these circuits and their link with apathy levels in the general population. We recruited 45 healthy subjects and measured their apathy scores using a dedicated questionnaire[18,19] as well as their valuation of efforts and rewards, using computational phenotyping of their behavior in an effort-based decision-making task[10,11,52,53]. To measure structural connectivity, we acquired whole-brain DWI in each subject and performed streamline tractography on fronto-M1 and fronto-BG-M1 circuits originating from SMA and OFC. For effective connectivity, we used ppTMS and probed these same circuits, as well as intra-M1 GABAa, GABAb, and glutamatergic circuits connecting to corticospinal neurons, providing a detailed, mechanistic characterization of these circuits up to the final motor neurons of the brain. Overall, our data characterizes fronto-motor connectivity changes associated with different aspects of subclinical apathy and effort-based decision processes in the healthy population, paving the way for their targeted neuromodulation in populations of patients suffering from apathy.

RESULTS

The study involved 45 healthy right-handed participants (25.1 ± 0.8 years old, 31 females, 14 males). We conducted a comprehensive neuropsychological assessment that included apathy scores (presented in Figure 1.A), as well as control variables related to apathy, such as depression and anhedonia scores (presented in Supplementary Figure 1). Apathy scores ranged between 0.54 and 1.92 (Figure 1.A), consistent with previous studies using the same scale in healthy individuals[18,54,55], namely the extended version of the Lille Apathy Rating Scale (LARS-e)[18]. Higher scores indicated stronger apathy.

A possible limitation of apathy scales is their reliance on subjective psychological constructs[10]. To complement our evaluation of motivated behavior, we employed a computational phenotyping approach to objectively characterize variability in effort-based decision-making processes previously linked to apathy in multiple pathologies[2,4–6,10,11,56] (Figure 1; see Supplementary Figure 2 for model selection and quality of fit data). Participants performed an effort-based decision-making task, requiring them to decide whether to exert varying levels of effort with their right arm (biceps contraction) to earn monetary rewards. We modelled participants' acceptance rates (presented in Supplementary Figure 2) to estimate two key parameters: β_{Effort}, reflecting effort valuation, and β_{Reward}, reflecting reward valuation[6,11,56]. Notably, high β_{Effort} and low β_{Reward} values are particularly relevant as they reflect high valuation of effort costs and low valuation of rewards, both of which are associated with reduced engagement in goal-directed behaviors[6,11,56]. While these computational parameters offer an objective, model-based way to capture variability in effort-based decision-making processes, a Bayes Factor (BF) regression analysis provided evidence for a lack of correlation between β_{Effort} / β_{Reward} and apathy scores (Supplementary Figure 3), consistent with prior work[10]. This suggests that effort-based decision-making offers a complementary approach that evaluates distinct dimensions of motivated behavior, not captured by apathy questionnaires in healthy subjects.

For structural connectivity, we acquired whole-brain DWI and performed streamline tractography[48,49] (Figure 1C). We examined all tracts connecting the SMA and OFC to M1, both directly and through the BG structures identifiable using our atlas, all within the left hemisphere. The BG structures included the dorsal and ventral Caudate (d-

and vCaudate), dorsolateral and ventromedial Putamen (dl- and vmPutamen), and the Nucleus Accumbens (NAcc). We also included the motor part of the thalamus to ensure the completeness of the circuits projecting to M1. We extracted the number of streamlines in each subject for 19 pairs of structures (detailed in Figure 2). A higher number of streamlines between two structures in one subject compared to another, reflects a greater probability that the fibers linking these two regions are more numerous, occupy a larger volume, or are in better condition and thus indicate a greater structural connectivity.

For effective connectivity, we used ppTMS (Figure 1D), which involved administering a test stimulation over the left M1, preceded by a conditioning stimulation in some trials[38,50,51,57]. We recorded the motor evoked potentials (MEPs) induced by the test stimulation with electromyography. We calculated a ratio of MEPs for trials with both conditioning and test stimulations to trials with test stimulations only. A larger MEP ratio (> 1) indicates a stronger facilitatory drive from the pre-activated circuit to M1[38,50,51,57]. We used an individualized, neuronavigated dual-coil approach to investigate circuits from SMA and from the frontopolar portion of OFC to M1 in the left hemisphere. We used short (7 ms) and long (15 ms) inter-stimulation intervals to probe short-latency and long-latency circuits, involving preferentially fronto-M1 and fronto-BG-M1 circuits, respectively[51,57]. We also used a single-coil approach to examine intra-M1 circuits. By varying inter-stimulation intervals and stimulation intensities with the single-coil approach, we probed preferentially intra-M1 GABAa, GABAb, and glutamatergic circuits[38,50].

Our study aimed to identify which independent variables quantifying structural connectivity (number of streamlines in 19 tracts) and effective connectivity (MEP ratios) are associated with three dependent variables: apathy scores, β_{Effort} and β_{Reward}. We employed a conservative two-step statistical approach. First, we used Least Absolute Shrinkage and Selection Operator (LASSO) regression, a penalized least squares method that selects relevant independent variables. LASSO can yield some regression coefficients (β coefficients) as zero. Only independent variables with non-zero regression coefficients are considered as associated with the dependent variable and thus selected. Second, we performed partial correlations between the dependent variables and the independent variables selected by the LASSO regression. This was

done to control for multiple potentially confounding variables that may covary with apathy and effort-based decision-making processes (*i.e.*, age, gender, depression, and anhedonia), ensuring that the associations we identified between apathy scores, β_{Effort}, and β_{Reward}, on the one hand, and structural or effective connectivity, on the other, were truly specific to the dependent variable considered.

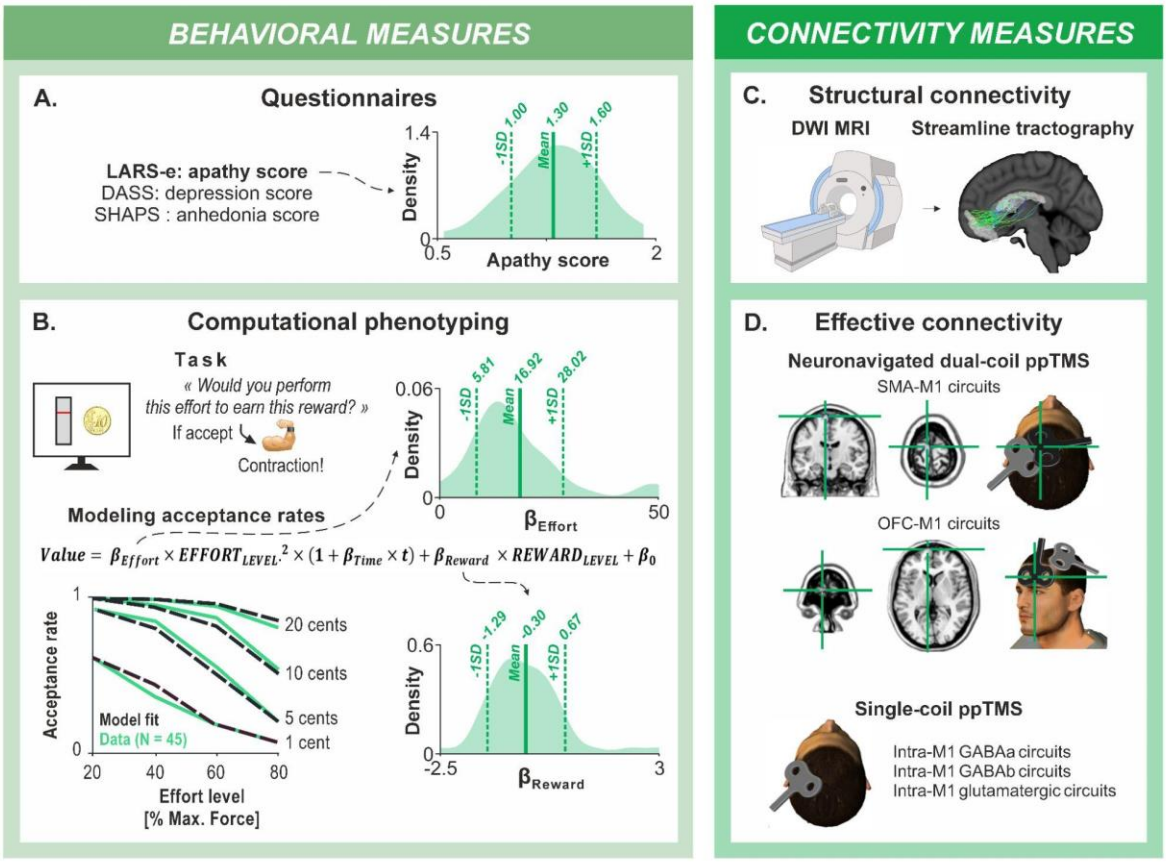

Figure 1. Behavioral and connectivity measures. A. Neuropsychological questionnaires: We conducted a comprehensive neuropsychological assessment, including the extended version of the Lille Apathy Rating Scale (LARS-e) to quantify apathy scores, as well as the Depression Anxiety Stress Scales (DASS) and the Snaith-Hamilton Pleasure Scale (SHAPS) to quantify depression and anhedonia scores, respectively. The density distribution on the right illustrates the high inter-individual variability in apathy scores among our group of 45 healthy subjects. The goal of the present study was to better understand this variability in apathy levels in the general population. **B. Computational phenotyping:** In the effort-based decision-making task (top left), participants decided whether to exert varying effort levels with their right biceps to earn different monetary rewards. The graph on the bottom left shows acceptance rates against effort levels for different monetary rewards for our sample of 45 subjects (green, solid line), also indicating our model fit to the data points (black, dashed line). Parameters β_{Effort} and β_{Reward} were estimated from the modeling of acceptance rates using the equation presented on top of the graph (see Supplementary Figure 1 for model comparison). Here again, the density distributions on the right depict the high inter-individual variability in β_{Effort} and β_{Reward} values among our group of 45 healthy subjects. **C. Structural connectivity:** We measured DWI on the 45 subjects and performed streamline tractography on circuits connecting the SMA, OFC, BG, and M1 within the left hemisphere. The number of streamlines

between pairs of structures was extracted for each subject, reflecting structural connectivity. **D. Effective connectivity:** We used a dual-coil ppTMS protocol (top) to measure effective connectivity in circuits from the SMA and OFC to M1. We employed an individualized, neuronavigated dual-coil approach to investigate circuits from the SMA and the frontopolar portion of the OFC to M1 in the left hemisphere. Short (7 ms) and long (15 ms) inter-stimulation intervals were used to probe short-latency and long-latency circuits (not represented here), preferentially involving fronto-M1 and fronto-BG-M1 circuits, respectively[51,57]. We used a single-coil ppTMS approach (bottom) to examine intra-M1 GABAa, GABAb, and glutamatergic intra-M1 circuits. MEPs were recorded, and MEP ratios were calculated to assess effective connectivity (not represented here). The head cartoons were created using Poser software, version 6.

Apathy scores are linked to connectivity in SMA-M1, SMA-BG and OFC-BG-M1 circuits

First, for structural connectivity, we performed a LASSO regression with the number of streamlines for the 19 tracts as independent variables and apathy scores as the dependent variable. The regression identified three tracts, namely SMA-M1, SMA-dlPutamen, and OFC-dCaudate, with non-zero coefficients, suggesting potential correlation with apathy scores (LASSO's β coefficients = 0.001, 0.00005, and 0.016, respectively; Figure 2.A). Partial correlation analysis confirmed significant positive correlations between apathy scores and the number of streamlines in these circuits, even when controlling for the potentially confounding variables ($R = 0.34$, $p = .028$; $R = 0.33$, $p = .033$; and $R = 0.39$ $p = .009$, respectively; Figure 2.B), indicating that higher apathy scores are associated with stronger structural connectivity in these circuits.

As highlighted above, LASSO regression is a penalized least squares method that eliminates irrelevant independent variables by reducing their regression coefficients to zero. To ensure no false negatives in LASSO's selection, we performed additional correlations with BF computation on non-selected tracts. This involved all other SMA-BG and OFC-BG circuits. The analysis confirmed no significant positive correlations between apathy scores and the number of streamlines in these alternative circuits (p-values range = [.437 .872] and [.199 .826] for SMA-BG and OFC-BG circuits, respectively). The BF_{01} for these correlations averaged 2.47 ± 0.05 (BF_{01} range = [1.78 3.24]), indicating a higher likelihood of no correlation for these circuits. This analysis confirms the absence of false negatives in LASSO's selection and emphasizes the circuit-specificity of the significant correlations.

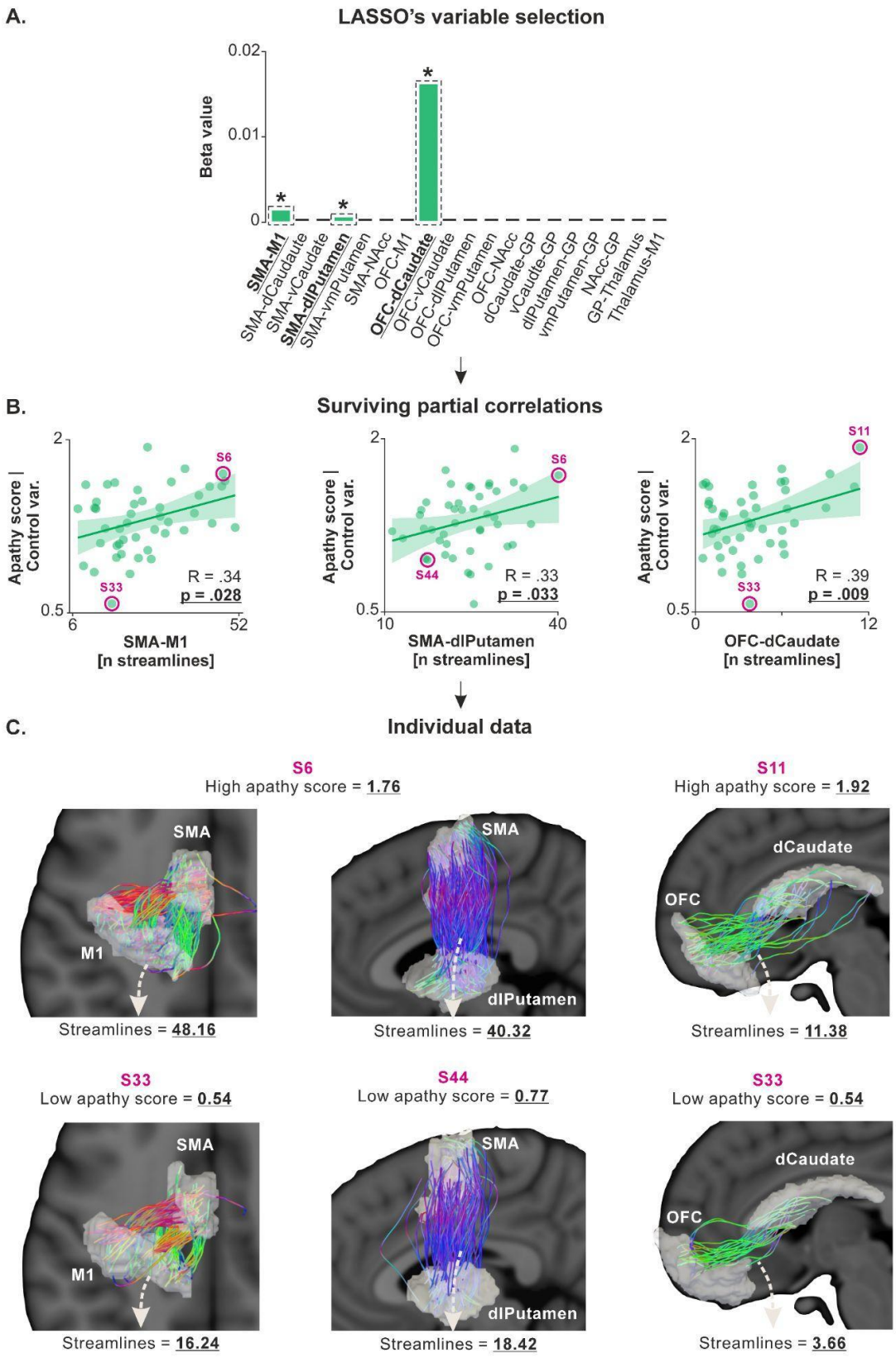

Figure 2. Apathy scores are linked to structural connectivity in SMA-M1, SMA-dlPutamen and OFC-dCaudate circuits. A. LASSO's variable selection. The bar graph shows the results of LASSO variable selection with structural connectivity data (*i.e.*, the

number of streamlines for the 19 tracts considered) as independent variables and apathy scores as the dependent variable. The regression identified three tracts (SMA-M1, SMA-dlPutamen, and OFC-dCaudate) with non-zero coefficients, suggesting a potential correlation with apathy scores. The green bar represents positive beta values, indicating a positive relationship with apathy scores. Bars highlighted by dashed black rectangles and a star indicate the independent variables that survived the ensuing partial correlation analysis. **B. Surviving partial correlations**. Partial correlation analysis confirmed significant positive correlations between apathy scores and the number of streamlines in these three circuits (x-axes), even when controlling for potential confounding variables (*i.e.*, apathy scores adjusted for age, gender, depression, and anhedonia on the y-axes). Higher values on the x-axes reflect stronger structural connectivity in the considered circuit. Similarly, higher values on the y-axes reflect higher apathy scores. **C. Individual data.** Subjects with high apathy scores (top row, S6 and S11) and low apathy scores (bottom row, S33 and S44) were selected from the correlations presented in the middle panel, and their white matter for the three selected circuits were plotted. Note that the regions of interest have been inflated for the streamline analysis and are thus inflated in this visual representation as well. This representation highlights the strong heterogeneity in structural connectivity, even within a sample of healthy subjects, and its relationship with apathy scores.

Second, for effective connectivity, we applied LASSO regression with all MEP ratios as independent variables and apathy scores as the dependent variable. This included ratios for short- and long-latency SMA- and OFC-M1 circuits, as well as intra-M1 GABAa, GABAb, and glutamatergic circuits. The regression revealed two circuits (short- and long-latency OFC-M1) with non-zero coefficients (LASSO's β coefficients = -0.23 and 0.61, respectively; Figure 3.A). Importantly, partial correlation analyses confirmed a significant positive correlation for the long-latency OFC-M1 circuit ($R = 0.38$, $p = .014$; Figure 3.B), indicating that higher apathy scores are associated with a stronger facilitatory influence of OFC on M1 (*i.e.*, MEP ratios > 1) in this long-latency circuit. However, this was not the case for the short-latency OFC-M1 circuit ($R = -0.09$, $p = .571$; Supplementary Figure 4).

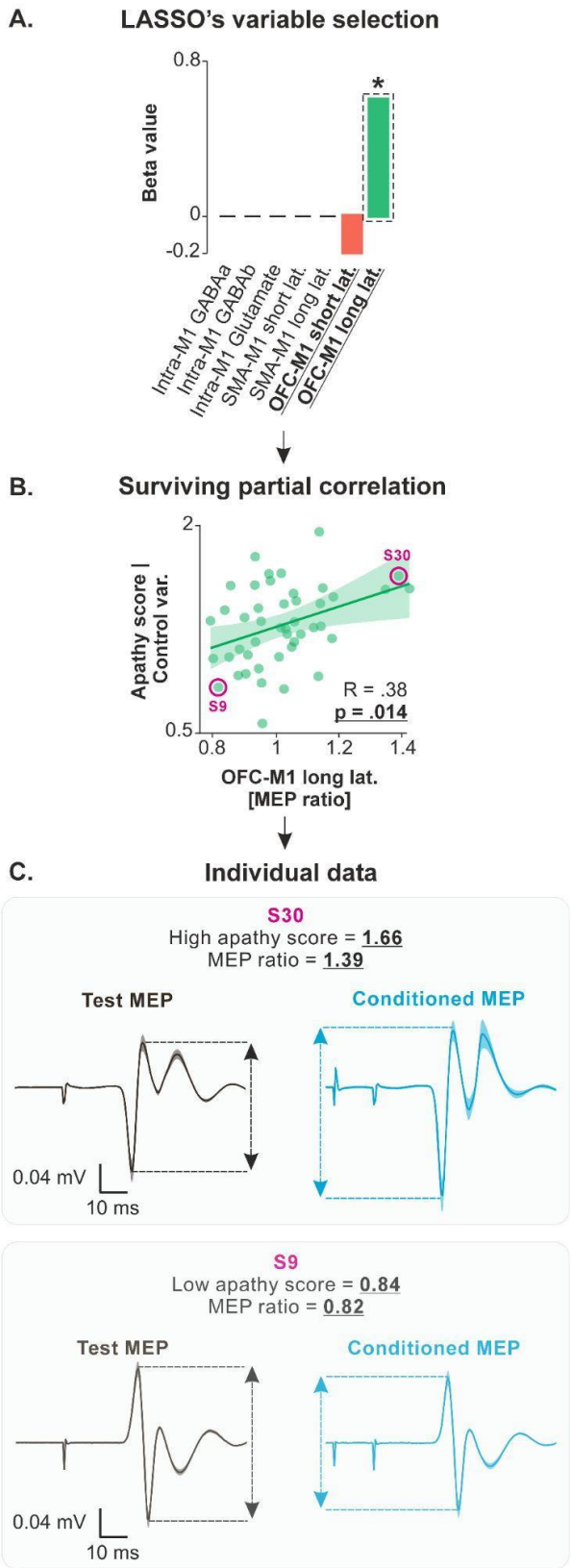

Figure 3. Apathy scores are linked to effective connectivity in the long-latency OFC-M1 circuit. A. LASSO's variable selection. The bar graph shows the results of LASSO variable selection, with effective connectivity data (*i.e.*, the MEP ratios) as independent variables and apathy scores as the dependent variable. The regression identified two circuits (short- and

long-latency OFC-M1 circuits) with non-zero coefficients, suggesting a potential correlation with apathy scores. The red and green bars represent negative and positive beta values, indicating negative and positive relationships with apathy scores. The bar highlighted by a dashed black rectangle and a star indicates the independent variable that survived the ensuing partial correlation analysis. **B. Surviving partial correlation**. Partial correlation analysis confirmed significant positive correlations between apathy scores and MEP ratios for the long-latency OFC-M1 circuits (x-axes), even when controlling for potential confounding variables (*i.e.*, apathy scores adjusted for age, gender, depression, and anhedonia on the y-axes). However, this was not the case for the short-latency OFC-M1 circuit ($R = -0.09$, $p = .571$; Supplementary Figure 4). Higher values on the x-axis (MEP ratios > 1) reflect stronger facilitatory influence of OFC on M1. Similarly, higher values on the y-axes reflect higher apathy scores. **C. Individual data.** Subjects with high apathy scores (top row, S30) and low apathy scores (bottom row, S9) were selected from the correlations presented in the middle panel, and their MEPs were plotted. The plots represent the average MEPs time-locked to the TMS pulse; shaded errors represent standard errors. Test MEPs were obtained with a single test stimulation over M1 while conditioned MEPs were obtained by first applying a conditioning stimulation on OFC, 15 ms before the test stimulation. S30 (top row) presents a high apathy score and a larger conditioned MEP amplitude relative to test MEP amplitude. Conversely, S9 (bottom row) presents a low apathy score and a tendency for a lower conditioned MEP amplitude relative to test MEP amplitude. These plots highlight the strong heterogeneity in effective connectivity between OFC and M1, even within a sample of healthy subjects, and its relationship with apathy scores.

Hence, our findings establish a link between apathy scores and connectivity in different SMA and OFC circuits connecting in part to M1. Notably, apathy scores showed a positive correlation with both structural and effective connectivity in OFC-BG-M1 circuits. However, the association observed with structural connectivity in SMA-M1 and SMA-dlPutamen circuits did not extend to effective connectivity. All observed correlations were positive, indicating that higher levels of apathy are associated with a stronger structural connectivity in these circuits and a stronger facilitatory influence from OFC to M1. This aligns with previous reports linking high subclinical apathy levels to increased activation[18] and hyperconnectivity[58] in frontal structures.

Effort valuation is linked to structural connectivity in SMA-M1 and SMA-BG circuits

We aimed to characterize the brain circuits associated with increasing β_{Effort} values. High β_{Effort} values are of particular interest because they reflect a stronger reduction in acceptance rates as effort levels increase. In other words, high β_{Effort}

values indicate a greater sensitivity to effort costs, which is linked to reduced engagement in effortful tasks[6,11,18].

The relationship between connectivity and effort valuation was analyzed using the same statistical procedure as for apathy scores. First, we performed a LASSO regression, with the number of streamlines for the 19 tracts as independent variables and β_{Effort} as the dependent variable. The regression identified seven tracts with non-zero coefficients: SMA-M1 (LASSO's β = 0.21), SMA-dlPutamen (β = -0.02), SMA-vmPutamen (β = -0.31), SMA-NAcc (β = -0.25), vCaudate-GP (β = -0.04), NAcc-GP (β = -0.11) and GP-Thalamus (β = 0.02; Figure 4.A). Partial correlation analyses confirmed significant correlations between β_{Effort} and the number of streamlines in three of these seven tracts, namely SMA-M1 (R = 0.42, p = .006), SMA-NAcc (R = -0.32, p = .042) and NAcc-GP circuits (R = -0.41, p = .007; Figure 4.B). As indicated by the sign of the R-values, the correlation with the number of streamlines in SMA-M1 circuit was positive while the correlations with SMA-NAcc and NAcc-GP circuits were negative, indicating that higher levels of effort valuation are associated with stronger cortico-cortical connectivity and weaker cortico-subcortical connectivity in SMA-related circuits. Other partial correlations were not significant and are presented in Supplementary Figure 5 (p-values range = [.198 .784]).

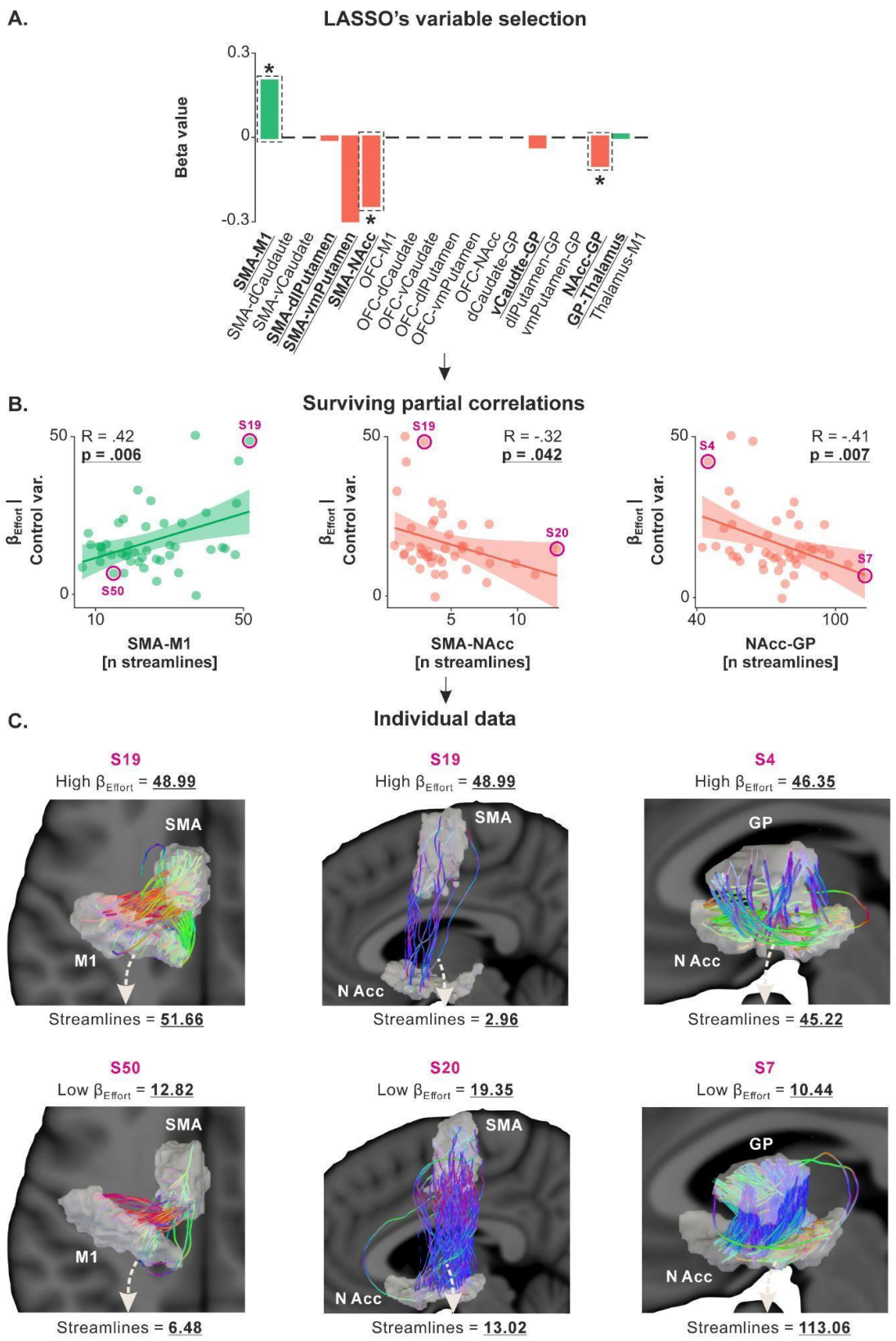

Figure 4. β_{Effort} is linked to structural connectivity in SMA-M1, SMA-NAcc and NAcc-GP circuits. A. LASSO's variable selection. The bar graph shows the results of LASSO variable selection, with structural connectivity data (*i.e.*, the number of streamlines for the 19 tracts considered) as independent variables and β_{Effort} as the dependent variable. The regression identified seven tracts (SMA-M1, SMA-dlPutamen, SMA-vmPutamen, SMA-NAcc, vCaudate-

GP, NAcc-GP and GP-Thalamus) with non-zero coefficients, suggesting a potential correlation with β_{Effort}. The red and green bars represent negative and positive beta values, indicating negative and positive relationships with β_{Effort}. Bars highlighted by dashed black rectangles and a star indicate the independent variables that survived the ensuing partial correlation analysis. **B. Surviving partial correlations***.* Partial correlation analysis confirmed significant correlations between β_{Effort} and the number of streamlines in three of the seven circuits (x-axes), even when controlling for potential confounding variables (*i.e.*, β_{Effort} adjusted for age, gender, depression, and anhedonia on the y-axes). Higher values on the x-axes reflect stronger structural connectivity in the considered circuit. Similarly, higher values on the y-axes reflect higher β_{Effort}, indicating stronger valuation of efforts in the effort-based decision-making task. Other partial correlations were not significant and are presented in Supplementary Figure 5 (p-values range = [.198 .784]). **C. Individual data.** Subjects with high β_{Effort} (top row, S19 and S4) and low β_{Effort} (bottom row, S50, S20 and S7) were selected from the correlations presented in the middle panel, and their white matter for the three selected circuits were plotted. Note that the regions of interest have been inflated for the streamline analysis and are thus inflated in this visual representation as well. This representation highlights the strong heterogeneity in structural connectivity, even within a sample of healthy subjects, and its relationship with β_{Effort}.

Second, we applied LASSO regression with MEP ratios as independent variables and β_{Effort} as the dependent variable. The regression yielded zero coefficients for all circuits (*i.e.*, all $\beta = 0$), signifying a lack of association between β_{Effort} and effective connectivity in the investigated circuits. All graphs depicting the results of the LASSO regression as well as the absence of significant partial correlation between all effective connectivity data and β_{Effort} are provided in Supplementary Figure 6 (p-values range = [.385 .887]).

Hence, our findings establish a link between effort valuation and structural connectivity in different SMA-related – and not OFC-related – circuits, in line with the well-known role of SMA in effort valuation[27,28]. However, as for apathy scores, the associations observed with structural connectivity in SMA-related circuits did not extend to effective connectivity alterations, in line with the idea that structural and effective connectivity measures provide complementary insights into neural circuits and do not necessarily co-vary with one another. Further, the correlation was positive for the SMA-M1 circuit and negative for SMA-NAcc and NAcc-GP circuits, indicating that effort valuation might be associated with different alterations in distinct fronto-motor circuits.

Reward valuation is linked to structural connectivity in a BG circuit and to effective connectivity in intra-M1 GABAa and GABAb circuits

We aimed to characterize the brain circuits associated with decreasing β_{Reward} values. Low β_{Reward} values are of particular interest because they reflect a lower increase in acceptance rates as reward levels increase. In other words, low β_{Reward} values indicate a lower sensitivity to rewards, which is linked to reduced engagement in effortful tasks[6,10,56].

The relationship between connectivity and reward valuation was analyzed using the same statistical procedure as for the other dependent variables. First, we performed the LASSO regression, with the number of streamlines for the 19 tracts as independent variables and β_{Reward} as the dependent variable, and identified one tract with a non-zero coefficient (NAcc-GP, LASSO's β coefficient = -0.012; Figure 5.A). The partial correlation analysis confirmed the presence of a significant negative correlation between β_{Reward} and the number of streamlines in the NAcc-GP circuits ($R = -0.42$, $p = .006$; Figure 5.B), consistent with the well-identified role of NAcc in value computation[59,60]. As such, the negative correlation indicates that lower β_{Reward} parameters – *i.e.*, lower levels of reward valuation – are associated with stronger structural connectivity in this circuit.

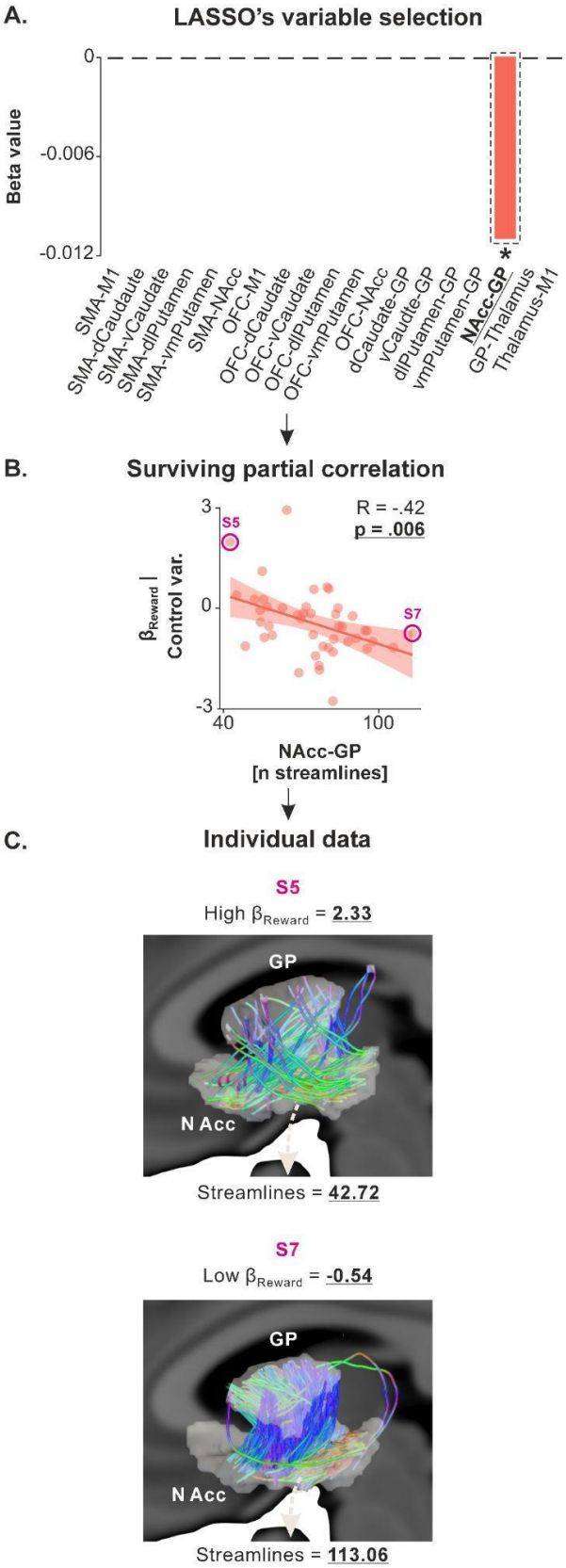

Figure 5. β_{Reward} is linked to structural connectivity in the NAcc-GP circuit. A. LASSO's variable selection. The bar graph shows the results of LASSO variable selection, with structural connectivity data (*i.e.*, the number of streamlines for the 19 tracts considered) as

independent variables and β_{Reward} as the dependent variable. The regression identified one tract (NAcc-GP) with a non-zero coefficient, suggesting a potential correlation with β_{Reward}. The red bar represents a negative beta value, indicating a negative relationship with β_{Reward}. This bar is highlighted by a dashed black rectangle and a star, indicating that it survived the ensuing partial correlation analysis. **B. Surviving partial correlation**. Partial correlation analysis confirmed the presence of a significant negative correlation between β_{Reward} and the number of streamlines in the NAcc-GP circuits (x-axes), even when controlling for potential confounding variables (*i.e.*, β_{Reward} adjusted for age, gender, depression, and anhedonia on the y-axes). Higher values on the x-axes reflect stronger structural connectivity in the NAcc-GP circuit. Further, lower values on the y-axes reflect lower β_{Reward}, indicating lower valuation of rewards in the effort-based decision-making task. **C. Individual data.** Subjects with high β_{Reward} (top row, S5) and low β_{Reward} (bottom row, S7) were selected from the correlations presented in the middle panel, and their white matter for the NAcc-GP circuit were plotted. Note that the regions of interest have been inflated for the streamline analysis and are thus inflated in this visual representation as well. This representation highlights the strong heterogeneity in structural connectivity, even within a sample of healthy subjects, and its relationship with β_{Reward}.

We then applied the LASSO regression with all MEP ratios as independent variables and β_{Reward} as the dependent variable and identified five circuits with non-zero coefficients (Figure 6.A): intra-M1 GABAa (LASSO's β = -0.015), intra-M1 GABAb (β = -0.006), intra-M1 glutamatergic (β = 0.002), short-latency OFC-M1 (β = 0.005) and long-latency OFC-M1 circuits (β = -0.0004). Partial correlation analyses confirmed the presence of a significant correlation between β_{Reward} and two of the five circuits, namely intra-M1 GABAa (R = -0.50, p = .0007) and intra-M1 GABAb circuits (R = -0.31, p = .047; Figure 6.B), two circuits that are known to be modulated during reward-based tasks[61,62]. As indicated by the sign of the R-values, the correlations between β_{Reward} and effective connectivity in intra-M1 GABAa and GABAb circuits was negative. The negative correlations indicate that participants with lower β_{Reward}, reflecting lower sensitivity to rewards (*i.e.*, those at the bottom of the y-axis in Figure 6.B), had reduced effective connectivity in intra-M1 GABAa and GABAb circuits. Reduced effective connectivity suggests less inhibitory influence from these GABAergic circuits on corticospinal neurons (*i.e.*, a reduction in the suppressive effect of GABAa and GABAb circuits, seen on the right side of the x-axis in Figure 6.B). In simpler terms, individuals who placed a lower value on rewards exhibited less GABA-mediated inhibition within M1. The other partial correlations were not significant and are presented in Supplementary Figure 7 (p-values range = [.101 .907]).

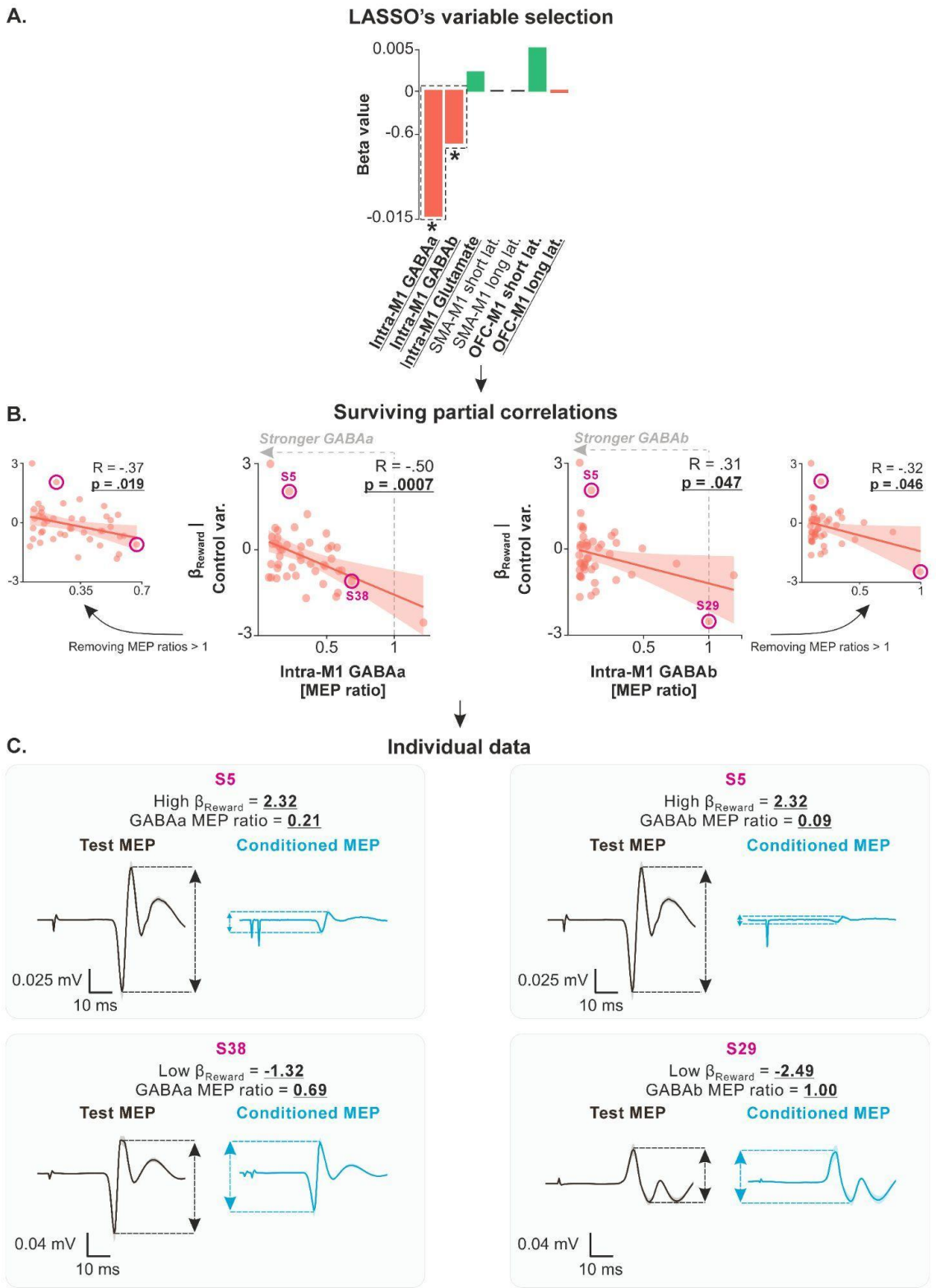

Figure 6. β_{Reward} is linked to effective connectivity in intra-M1 GABAa and GABAb circuits. A. LASSO's variable selection. The bar graph shows the results of LASSO variable selection, with effective connectivity data (*i.e.*, the MEP ratios) as independent variables and

β_{Reward} as the dependent variable. The regression identified five circuits tracts with non-zero coefficients, suggesting a potential correlation with β_{Reward}. The red and green bars represent negative and positive beta values, indicating negative and positive relationships with apathy scores. Bars highlighted by dashed black rectangles and a star indicate the independent variables that survived the ensuing partial correlation analysis. **B. Surviving partial correlations***.* Partial correlation analysis confirmed significant negative correlations between β_{Reward} and MEP ratios for two of the five circuits: intra-M1 GABAa (R = -0.50, p = .0007) and intra-M1 GABAb circuits (x-axes), even when controlling for potential confounding variables (*i.e.*, β_{Reward} adjusted for age, gender, depression, and anhedonia on the y-axes). Other partial correlations were not significant and are presented in Supplementary information 6 for the sake of transparency (p-values range = [.101 .907]). Lower values on the x-axis (MEP ratios < 1 and tending toward 0) reflect stronger suppressive influence of the GABAa and GABAb circuits on corticospinal neurons. Additionally, lower values on the y-axes reflect lower β_{Reward} and thus a lower valuation of rewards in the effort-based decision-making task. **C. Individual data.** Subjects with high β_{Reward} (top row, S5) and low β_{Reward} (bottom row, S38 and S29) were selected from the correlations presented in the middle panel, and their MEPs were plotted. The plots represent the average MEPs time-locked to the TMS pulse; shaded errors represent standard errors. Test MEPs were obtained with a single test stimulation over M1 while conditioned MEPs were obtained by first applying a conditioning stimulation on M1 before the test stimulation. S30 (top row) presents a high β_{Reward} and a strong suppression of conditioned MEP amplitude relative to test MEP amplitude both for GABAa and GABAb circuits, indicating a strong effective, suppressive influence of these circuits on corticospinal neurons. Conversely, S38 and S29 (bottom row) presents a low β_{Reward} and almost no suppression of conditioned MEP amplitudes relative to test MEP amplitudes, indicating a weak suppressive influence of GABA circuits on corticospinal neurons. These plots highlight the strong heterogeneity in effective connectivity in intra-M1 GABAa and GABAb circuits, even within a sample of healthy subjects, and its relationship with β_{Reward}.

Hence, our findings establish a link between reward valuation and structural connectivity in an isolated tract of the BG circuitry – *i.e.*, the NAcc-GP tract. Interestingly, this tract's connectivity is also tied to effort valuation, supporting the NAcc's role in integrating reward and effort values to compute the net value of actions[13,34,63]. We also found a negative link between reward valuation and effective connectivity in intra-M1 GABAa and GABAb circuits. This means lower reward valuation is linked to less inhibition of corticospinal neurons by these circuits, aligning with literature showing GABAergic circuits' role in reward-based behaviors[61,62]. A summary of the correlations we uncovered is presented in Figure 7.

A.

Behavioral measures	Structural connectivity	Effective connectivity
Apathy scores	OFC-dCaudate, SMA-M1, SMA-dlPutamen	Long-latency OFC-(BG)-M1
Effort valuation	SMA-M1, SMA-NAcc, NAcc-GP	None
Reward valuation	NAcc-GP	Intra-M1 GABAa and GABAb

B.

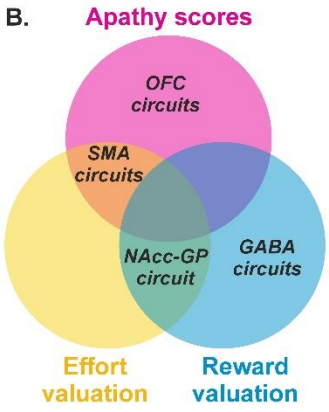

Figure 7: Summary of the main correlations uncovered in the present study. A. Detailed correlations. Green and red colors are used to highlight positive and negative correlations, respectively. Apathy scores are linked to structural connectivity in the SMA-M1, SMA-dlPutamen, and OFC-dCaudate circuits, as well as to long-latency OFC-M1 effective connectivity. Effort valuation is associated with structural connectivity in the SMA-M1, SMA-NAcc, and NAcc-GP circuits. Reward valuation is linked to structural connectivity in the NAcc-GP circuit and effective connectivity in intra-M1 GABAergic circuits. **B. Overlapping and specific circuits .** This Venn diagram provides an overview of the circuits shared and specific to apathy scores, effort valuation, and reward valuation.

Apathy scores, effort valuation and reward valuation are not linked to M1 net output

The data presented above show correlations between apathy scores, β_{Effort} and β_{Reward}, on the one hand, and both structural and effective connectivity, on the other, including circuits projecting to and within M1. Given this, it is possible that variability in connectivity towards M1 could lead to differences in M1's net neural output across apathy scores, β_{Effort} and β_{Reward} values. If that were the case, M1 net output would be, by itself, linked to apathy scores, β_{Effort}, and β_{Reward}.

To test this idea, we performed partial correlations with apathy scores, β_{Effort}, and β_{Reward} as dependent variables and test MEP amplitudes (obtained with a single test stimulation over M1), a proxy for M1 net output, as the independent variable. Control variables included age, gender, depression, and anhedonia. Partial correlations showed no significant link between apathy scores ($R = -0.11$, $p = .468$), β_{Effort} ($R = 0.05$, $p = .737$), β_{Reward} ($R = -0.12$, $p = .446$) and test MEP amplitudes (Supplementary Figure 8). BF computation indicated a higher likelihood of no correlation (BF_{01} averaged 2.59 ± 0.34, range = [2.12 - 3.25]).

Thus, despite correlations between apathy scores, effort valuation, reward valuation, and connectivity in circuits projecting to M1, these dependent variables are not linked to M1 net output alone. This analysis is also an important methodological control as it shows that the relationships between apathy scores, β_{Effort}, β_{Reward}, and MEP ratios are not due to associations with the test MEP amplitudes exploited to compute these ratios.

DISCUSSION

This study explored the relationship between apathy and effort-based decision-making, and connectivity in circuits linking key fronto-BG structures to M1. Our data showed that different variables characterizing apathy and effort-based decision-making processes – namely apathy scores, β_{Effort}, and β_{Reward} – were linked to distinct brain circuits, some of which project to M1. First, apathy scores were linked to connectivity in both SMA- and OFC-originating circuits. Specifically, our tractography data showed stronger structural connectivity in SMA-M1, SMA-BG, and OFC-BG circuits as apathy scores increases. Additionally, ppTMS data highlighted a positive correlation between facilitatory long-latency OFC-M1 effective connectivity and apathy scores, likely mediated by an OFC-BG-M1 circuit. Second, effort valuation was linked exclusively to SMA-related circuits. Individuals with higher β_{Effort} showed stronger structural connectivity in SMA-M1 and SMA-BG circuits, supporting the known role of SMA in effort valuation. Lastly, reward valuation was associated with structural connectivity in the NAcc-GP BG tract, with lower β_{Reward} (indicative of a reduced engagement for increasing rewards) observed in subjects showing stronger connectivity. Finally, lower β_{Reward} was also associated with lower effective connectivity in intra-M1 GABAergic circuits.

Interestingly, much of the relationships we uncovered suggest that reduced engagement in effort (*i.e.*, higher apathy scores, higher β_{Effort}, and lower β_{Reward}) is linked to stronger structural and effective connectivity. This applies across several circuits, including SMA- and OFC-originating circuits (higher apathy), the SMA-M1 circuit (higher effort valuation), and the NAcc-GP circuit (lower reward valuation). At first glance, these findings may seem at odds with the well-known link between both

subclinical and clinical apathy and brain abnormalities such as grey matter atrophy[32,64–66], hypoactivation[67], hypometabolism[68], white matter lesions[18,64], and reduced functional connectivity[25,69,70]. However, some studies have also reported high subclinical apathy levels associated with increased activation[18] and hyperconnectivity[58] within frontal structures.

Our findings can be interpreted in two ways. First, increased connectivity in these circuits might be detrimental to effort-based decision-making. High functional or effective connectivity at rest may reduce the brain's ability to adjust dynamically to different effort and reward magnitudes during decision-making. This kind of hyperconnectivity is seen in various disorders where different aspects of motivated behavior are affected. For instance, schizophrenia is associated with both negative symptoms, such as avolition and asociality, and increased functional connectivity[71]. Depression is linked to both anhedonia and an expansion of brain networks[72] as well as hyperconnectivity in specific brain networks[73–75]. In Parkinson’s disease, patients exhibit reduced movement vigor and excessive beta band connectivity in fronto-BG circuits[76–78]. On the other hand, heightened connectivity might help rather than hinder. It could enhance neural communication during effort-based decisions, helping individuals with subclinical apathy to avoid tipping into clinical apathy. For example, in traumatic brain injury patients, those who show high subclinical apathy levels have hyperconnectivity in frontal circuits, while those who develop clinical apathy show reduced connectivity in these same circuits[58]. This suggest that hyperconnectivity could reflect an initial stage of compensation in specific fronto-motor circuits in individuals with mild apathy that is ultimately insufficient as the pathology progresses[58]. If this is correct, the relationship between connectivity and apathy might follow a non-linear path in certain circuits. Starting with normal connectivity at low apathy levels, it could progress to hyperconnectivity at higher subclinical levels, and eventually to hypoconnectivity in more severe, clinical cases. Understanding this dynamic could pave the way for developing diagnostic biomarkers that track different stages of apathy across individuals, and design stage-dependent neuromodulation approaches.

Among the positive correlations we found, apathy scores were linked to connectivity in several circuits originating from both SMA and OFC, partially projecting

to M1. This finding is significant for two reasons. First, it contrasts with the more specialized circuits involved in effort valuation (SMA circuits) and reward valuation (NAcc and GABAergic circuits). This supports the idea that apathy scores may capture broader processes driving motivated behavior[10], engaging multiple brain circuits with different roles. In contrast, effort and reward valuation, as captured by computational models, may engage more specific circuits. Second, it sheds light on M1, a region often overlooked in studies of effort-based decision-making and apathy. This oversight likely stems from the influence of serial decision-making models, which suggest that motor regions only come into play after a decision has been made, to execute movements[79,80]. However, research in rodents, non-human primates, and humans has consistently shown that M1 activity changes during decision-making, especially in response to effort and reward[39,41,44]. This supports the idea that decision-making relies on a distributed consensus across brain regions[36,38], with connectivity modulations within fronto-BG-M1 recurrent loops playing a more active role than previously thought[47,81]. On a practical level, the association of fronto-motor circuits including M1 with apathy opens new translational opportunities to modulate and probe these circuits using multifocal non-invasive brain stimulation techniques such as paired-associative TMS[82–84] or bifocal transcranial alternating current stimulation approaches[85]. Although our findings are correlational and based on structural and resting-state measures, they align with the idea that connectivity in fronto-BG-M1 circuits is crucial for multiple dimensions of apathetic behavior.

Higher effort valuation was also linked to stronger structural connectivity between SMA and M1, which was also associated with higher apathy scores. This correlation is interesting because SMA activity has been shown to scale with the intensity of muscle contraction[22,27], and disruption of the SMA alters effort perception[28,86]. This supports the idea that the SMA plays a key role in encoding effort costs[28,86]. Additionally, research on motor imagery suggests that SMA suppresses M1 activity when imagining movements without actually performing them[87]. One possibility is that stronger SMA-M1 connectivity enhances the SMA's ability to suppress motor activity when mentally simulating actions involving high efforts. Another possibility is that the increased connectivity we found stems from projections running in the opposite direction, from M1 to SMA, given that these regions are densely, reciprocally connected[88–90]. Our data showed no link between effort valuation or apathy scores

and short-latency effective connectivity from SMA to M1, suggesting that structural connectivity changes in SMA-M1 projections alone may not explain the observed effects. Stronger M1-SMA connectivity could allow M1 to communicate more efficiently the body's state to SMA, improving effort estimation during embodied decisions. Further research is needed to clarify the specific roles of SMA-M1 and M1-SMA circuits in effort valuation, and their relationship to apathy.

Our data also reveal that higher effort valuation is linked to weaker structural connectivity in the SMA-NAcc and NAcc-GP circuits. Interestingly, weaker NAcc-GP connectivity is also tied to higher reward valuation. In other words, individuals with weaker NAcc-GP connectivity are more sensitive to changes in both effort and reward. They reduce their acceptance rates more sharply as effort increases (higher β_{Effort}) and increase their acceptance rates more strongly with increasing rewards (higher β_{Reward}). This fits with the known role of the NAcc in computing the net value of actions, weighing effort and reward[34,63]. Further, the net impact of the NAcc-GP circuit on motor cortical output is mostly suppressive[91]. Indeed, the NAcc primarily projects through inhibitory medium spiny neurons to the pallidum[91–93], which in turn inhibits the suppressive influence of ventral mesencephalon structures on thalamo-cortical circuits via the so-called indirect pathway of the BG[91]. One possibility is that the weaker structural connectivity we found reflects fewer or altered axons of medium spiny neurons projecting from the NAcc to the pallidum. This could reduce their suppressive effect on motor output, making individuals more sensitive to changes in both effort and reward levels.

Finally, lower reward valuation was also linked to weaker GABAa and GABAb effective connectivity within M1. This effect was specific to GABAergic circuits and did not concern glutamatergic ones. Importantly, a similar finding is observed in people with major depression, who present lower plasma GABA levels compared to controls, indicating reduced inhibitory function in individuals with impaired motivation[94]. Further, in task settings, GABAergic neurons in M1 adjust their activity in response to reward cues and delivery[61,62], acting as a "brake" on motor output that is released when rewards are available. These findings, along with our data, suggest that GABAergic circuits may play a role in regulating reward-driven behavior down to the final motor neurons of the brain. Specifically, the present study suggests a possible compensatory

mechanism: individuals with higher reward valuation may develop more efficient inhibitory circuits to corticospinal neurons at rest, preventing triggering any action when high rewards are at stake. In contrast, those less sensitive to rewards may need less GABA-driven suppression of the motor system.

Overall, this study adds a missing piece to the puzzle of the apathy network. It reveals clear links between apathy levels and effort-based decision-making processes in the general population on the one hand, and specific fronto-BG circuits on the other, including some directly connected to the brain's output neurons in M1. These results also underscore the value of combining a detailed assessment of motivated behavior, including well-established computational approaches, with multimodal connectivity measures to better understand the neural mechanisms underlying apathy.

ACKNOWLEDGMENTS

GD was supported by a FNRS Research associate grant. P.V. was supported by the Fund for Research training in Industry and Agriculture (FRIA/FNRS; FC29690) and grants by the Platform for Education and Talent (Gustave Boël—Sofina Fellowships), Wallonie-Bruxelles International. JD was supported by three FNRS research grants (T008219F, J005921F and T007023F). We would like to thank Matthieu Boisgontier, Ahmad Noureddine and Valentin Touzé for their participation in data acquisition.

AUTHOR CONTRIBUTIONS

GD: study conception, data acquisition, TMS data processing, statistical analysis, interpretation of the results, article writing from the first draft to the final version. PV: computational modelling, interpretation of the results, article writing. LD, QD, ND: MRI data processing, article writing. AZ: computational modelling, interpretation of the results, article writing. JD: study conception, interpretation of the results, article writing.

DECLARATION OF INTERESTS

The authors declare no competing interests.

MATERIALS AND METHODS

Resource availability

Lead Contact

Further information and requests for resources can be directed to and will be fulfilled by the corresponding author, Gerard Derosiere: gerard.derosiere@inserm.fr.

Data and Code Availability

- Data availability: all datasets will be freely available on the Open Science Framework repository upon publication, at: https://osf.io/a59mt/.
- Custom code availability: all custom codes generated during this study will be freely available on the Open Science Framework repository upon publication, at: https://osf.io/a59mt/.
- Any additional information required to reanalyze the data reported in this work paper is available from the lead contact upon request.

Experimental Model and Subject Details

The study initially involved 50 healthy human subjects recruited from the Research Participant Pool at the Institute of Neuroscience of UCLouvain. However, the experimental design consisted of two sessions and 3 out of the 50 subjects did not attend the second session. Additionally, tractography analysis could not be performed on 2 subjects due to corrupted MRI data. Consequently, the results presented in this article focus on the data of the 45 remaining subjects (25.1 ± 0.8 years old, 31 females, 14 males).

All subjects were right-handed according to the Edinburgh Questionnaire (Oldfield, 1971). None of the participants had any neurological disorder or history of psychiatric

illness or drug or alcohol abuse, or were on any drug treatments that could influence performance. Participants were financially compensated for their participation and earned additional money depending on their performance on the task (see below). The protocol was approved by the institutional review board of the Université catholique de Louvain, Brussels, Belgium, and required written informed consent.

Method details

The study consisted of two sessions, conducted with a minimum interval of 24 hours and a maximum interval of one week. The first session involved MRI data acquisitions and was performed at the Saint-Luc University Hospitals (Brussels, Belgium). The second session involved TMS data acquisition, behavioral data acquisition on the effort-based decision-making task, and the administration of a battery of neuropsychological questionnaires (*i.e.*, systematically realized in this order). It was performed at the Institute of Neuroscience of UCLouvain in Brussels. Below, we provide specific details for each of these acquisitions.

Magnetic Resonance Imaging

A 3D T1-weighted image was acquired for each participant on a 3T GE SIGNA™ Premier scanner (GE Healthcare, Chicago, IL) with the following parameters: Echo Time (TE) = 2.96 ms, Repetition Time (TR) = 2238.93 ms, Inversion Time (TI) = 900 ms, 170 slices, slice thickness: 1 mm,in-plane Field Of View (FOV): 256 × 256 mm², matrix size: 256x256, 1 mm isotropic. All participants also underwent a diffusion-weighted MRI scan with the following parameters: TR = 7289 ms, TE = 57.1 ms, 70 slices, slice thickness: 2 mm,, in-plane FOV: 220 × 220 mm², matrix size: 110x110, 2 mm isotropic voxels, 64 gradients at b = 1000 s/mm² , and one reference b0 image. Preprocessing of the diffusion data was performed using the Elikopy pipeline[95] and included brain extraction[96], thermal denoising [Veraart et al., 2016], susceptibility-induced distortions, eddy-current distortion and head-motion correction[97] using FSL (v6.0.7.8)[98]. Due to unavailability of an unweighted diffusion image with reversed

phase-encoding, Synb0-DISCO[99] was used to synthesize a distortion-free unweighted diffusion image from the T1-weighted image.

Dual-coil paired-pulse transcranial magnetic stimulation

General description

The dual-coil ppTMS setup involves administering a test stimulation (TS) with one coil over the primary motor cortex (M1), preceded by a conditioning stimulation (CS) delivered with another coil over a specific area of interest (*i.e.*, TS and CS coils, respectively). This technique enables the assessment of the impact of specific cortico-cortical and cortico-subcortico-cortical circuits on corticospinal neurons. Our objective was to investigate intra-hemispheric influences of the supplementary motor area (SMA) and orbitofrontal cortex (OFC) on M1. To achieve this, both stimulations were applied over the left, dominant hemisphere, with the TS targeted at the left M1 and the CS directed at either the left SMA or the left OFC in separate blocks of trials. We employed two small figure-of-eight coils (Magstim D25-Alpha model; wing internal diameter: 35 mm) connected to two monophasic Magstim stimulators (200^2 and Bistim^2 stimulators; Magstim, Whitland, Dyfed, UK) for delivering the TS and the CS.

TS coil location

We placed the TS coil tangentially on the scalp over the M1 area with the handle pointing backward and laterally at a 45° angle away from the midsagittal line, resulting in a postero-anterior current flow within the cortex[50,100]. To determine the optimal site for M1 stimulation, known as the "hotspot", we used markers on an electroencephalography (EEG) cap fitted on the participant's head[101–103]. Due to the close anatomical proximity of left M1 and left SMA, we had to slightly adjust the position of the M1 coil in 44 of the 47 subjects when the SMA coil was placed on the scalp; this adjusted position was used for TS during SMA blocks. Consequently, we defined two different positions for M1 stimulation: the real hotspot and an adjusted hotspot (see[51], for a similar procedure).

To locate the real hotspot, we initially applied the stimulation with the center of the TS coil over the C3 location of the EEG cap (*i.e.*, corresponding to the left M1 area)[104,105], without the presence of the CS coil on the head. We increased the stimulation intensity until consistent motor evoked potentials (MEP) were observed in the right first dorsal interosseous (FDI) muscle. We then moved the TS coil in increments of approximately 0.5 cm around this location in both the rostrocaudal and mediolateral axes. Stimulation was applied at the previously determined intensity at each new location and MEP amplitudes were visually assessed. The real hotspot was defined as the location where the largest and most consistent MEP amplitudes could be elicited. The coil was held in this position and the edges of its shape were marked on tapes placed on the EEG cap. These markings allowed us to locate the real hotspot throughout the experiment. To determine the adjusted hotspot, we positioned the CS coil over the SMA area on the head and then followed the same procedure as described above, while aiming at fitting both the TS and the CS coils on the head. After obtaining the largest MEP amplitudes, we marked the edges of the TS coil on the EEG cap. These markings enabled us to locate the adjusted hotspot during SMA blocks.

CS coil locations

To ensure precise targeting of SMA and OFC with the CS coil in each subject, we exploited neuronavigation. To do so, we used the T1-weighted high-resolution anatomical MRI data obtained in the first session (see MRI section, above). We determined the individual SMA and OFC locations on the MRI images, using Montreal Neurological Institute (MNI) coordinates in a dedicated software (Visor 2.0 Advanced NeuroTechnologies, Enschede, Netherlands). During the experiment, we relied on head and coil trackers, along with a 3D tracking device, to register the position of the CS coil with the individual MRI.

The MNI coordinates initially used to localize SMA and OFC were x = -8, y = -9, z = 77, and x = -7, y = 71, z = -4, respectively[106]. These coordinates were then slightly adjusted for each subject using the Visor software, ensuring they corresponded to the point where the scalp-to-cortex distance was minimal. Following this procedure, the

final MNI coordinates for SMA and OFC locations were x = -7.9 ± 0.2, y = -5.4 ± 0.5, z = 85.6 ± 0.7, and x = -8.3 ± 0.9, y = 72.9 ± 0.4, z = 2.5 ± 2.2, respectively.

For both SMA and OFC stimulations, the center of the CS coil was placed over the corresponding target location (see Figure 1.D). In SMA blocks, the CS coil was positioned tangentially to the scalp with the handle pointing at a -100° angle away from the midsagittal line (*i.e.*, in the counter-clockwise direction), resulting in a medio-lateral current flow within the cortex. This coil position was selected based on a previous experiment demonstrating optimal recruitment of SMA neurons. In OFC blocks, the CS coil was placed tangentially to the forefront, with the handle directed upward and parallel to the midsagittal line, leading to a downward current flow at the cortical level.

Stimulation intensities and inter-stimulation intervals

Once we defined the real and adjusted hotspots, we determined the resting motor threshold (rMT) for both locations. The rMT was defined as the lowest stimulation intensity (*i.e.*, expressed as a percentage of maximal stimulator output [% MSO]) required to evoke MEPs of 50 µV amplitude on 5 out of 10 consecutive trials in the relaxed FDI muscle. The rMTs for the real and adjusted hotspots were 46.7 ± 1.1 % and 50.8 ± 1.3 % MSO, respectively. These rMT values were used to determine the stimulation intensities for the rest of the experiment. In SMA blocks, we positioned the TS coil over the adjusted hotspot and based the stimulation intensity for M1 on the rMT obtained at this location; M1 was stimulated at 120 % of this rMT. Conversely, in OFC blocks, the TS coil was easily positioned over the real hotspot, allowing us to stimulate M1 at 120 % of the rMT obtained for the real hotspot. Finally, the CS intensity was set at 130 % and 120 % of the rMT obtained over the real hotspot in SMA and OFC blocks, respectively. We decided to apply a higher stimulation intensity over SMA based on previous studies using 140 % of the active motor threshold[107]. A slightly lower intensity was used over OFC to reduce facial contractions and subject discomfort.

The goal of the study was to investigate cortico-cortical and cortico-subcortico-cortical circuits between the SMA/the OFC and M1, which are assumed to be preferentially recruited with short (4-8 ms) and long (12-15 ms) inter-stimulation

intervals (ISIs), respectively[51,57]. Considering that 7 ms produces the best test-retest reliability when stimulating SMA[107], we decided to use a 7 ms ISI to probe cortico-cortical circuits. To assess the influence of cortico-subcortico-cortical circuits, we decided to use an ISI of 15 ms[51].

Blocks of trials

The dual-coil ppTMS protocol was divided into 4 blocks of 36 trials (*i.e.*, 2 SMA blocks and 2 OFC blocks). Each block comprised trials with single-pulse (*i.e.*, TS only) and paired-pulse TMS (*i.e.*, CS+TS with the intervals mentioned above), occurring in a randomized order. Within each block, a total of 12 trials were recorded for each of the 3 conditions (*i.e.*, single-pulse, and paired-pulse with 7 and 15 ms), leading to 24 trials per condition over the whole experiment. Finally, to prevent subjects from anticipating the stimulations, we varied the intertrial interval, which ranged between 3.6 and 4.4 s (*i.e.*, rectangular distribution centered over 4 s).

Single-coil ppTMS

General description and coil location

The single-coil ppTMS protocol was performed right after the dual-coil ppTMS protocol. Single-coil ppTMS involves administering a TS preceded by a CS through the same single coil, placed over M1. This technique enables the assessment of the impact of specific intra-cortical circuits on corticospinal neurons. Here, we did not use a small figure-of-eight coil because it lacks programmability and the ability to rapidly change stimulation intensity, which is necessary for single-coil ppTMS. Instead, we employed a large, programmable figure-of-eight coil (Magstim D25-Alpha model; wing internal diameter: 70 mm), which we connected to two the monophasic Magstim stimulators mentioned above (200[2] and Bistim[2] stimulators; Magstim, Whitland, Dyfed, UK) for delivering both the TS and the CS. To determine the optimal coil location in the single-coil setup, we followed the same procedure as the one utilized for identifying the real hotspot location in the dual-coil setup, employing the larger coil (*i.e.*, initial

targeting of the C3 location, displacement of the coil in increments of 0.5 cm, markings on the EEG cap, *etc*.).

Stimulation intensities and inter-stimulation intervals

The rMT for the single-coil setup was 46.5 ± 1.1 % MSO. Importantly, in single-coil ppTMS, both the intensity of the CS and the duration of the ISI play crucial roles in determining the specific subset of intra-cortical circuits under investigation. Certain variants of single-coil setups employ a subthreshold intensity for the CS, allowing the targeting of intra-cortical circuits with low activation thresholds (Daskalakis et al., 2002). At such intensities, using a short ISI ranging from 2 to 6 ms results in the suppression of the conditioned MEP, known as short-latency intra-cortical inhibition (SICI). This phenomenon is believed to be generated by low-threshold inhibitory circuits, involving fast γ-aminobutyric acid (GABA) synapses of the GABAa subtype (Di Lazzaro et al., 2006; Ilic et al., 2002). Conversely, combining a subthreshold conditioning pulse with a longer ISI ranging from 8 to 30 ms leads to the facilitation of the conditioned MEP, referred to as long-interval intra-cortical facilitation (LICF). This effect is thought to reflect the influence of glutamatergic projections on corticospinal neurons (Ziemann et al., 1998). Lastly, when a suprathreshold conditioning pulse is combined with a long ISI ranging from 50 to 200 ms, the MEP is suppressed again, giving rise to long-latency intra-cortical inhibition (LICI). This effect is believed to be mediated by high-threshold inhibitory circuits, primarily involving slow GABAb synapses (McDonnell et al., 2006).

In this study, our objective was to investigate these three distinct types of intra-cortical circuits. To probe GABAa circuits, we utilized a subthreshold CS intensity of 80 % rMT and a short ISI of 3 ms. To probe glutamatergic circuits, we employed a subthreshold CS intensity of 80 % rMT and a longer ISI of 10 ms. To probe GABAb circuits, we utilized a suprathreshold CS intensity of 120 % rMT and a long ISI of 100 ms. In all three cases, we elicited MEPs using a suprathreshold TS intensity of 120% rMT.

To validate that our single-coil approach effectively targeted the inhibitory and excitatory circuits under investigation, we analyzed the MEP amplitudes recorded in

TS-only trials and CS+TS trials across the different stimulation intensities and inter-stimulation intervals used. In TS-only trials, the MEP amplitude was 0.56 ± 0.08 mV. In CS+TS trials, the MEP amplitudes were 0.12 ± 0.05 mV for GABAa circuits, 0.02 ± 0.03 mV for GABAb circuits, and 0.72 ± 0.10 mV for glutamatergic circuits. As anticipated, this resulted in MEP ratios below 1 for GABAa and GABAb circuits (0.36 ± 0.03 and 0.16 ± 0.03, respectively) and above 1 for glutamatergic circuits (1.26 ± 0.07). These findings confirm the expected inhibitory and excitatory circuit responses.

Blocks of trials

The single-coil ppTMS protocol was divided into 2 blocks of 48 trials. Here again, each block comprised trials with single-pulse (*i.e.*, TS only) and paired-pulse TMS (*i.e.*, CS+TS), occurring in a randomized order and a total of 12 trials were recorded for each of the 4 conditions (*i.e.*, single-pulse, and paired-pulse for GABAa, GABAb, and glutamatergic circuits), leading to 24 trials per condition over the whole experiment. The intertrial interval ranged between 3.6 and 4.4 s.

Effort-based decision-making (EBDM) task

Experimental set-up

Following the TMS data acquisitions, subjects were invited to perform an EBDM task on a computer. To do so, they were seated in a comfortable chair positioned 100 cm away from the computer screen with a refresh rate of 100 Hz. Their right elbow was bent at a 90-degree angle, resting on an armrest, while they held a gripping handle with their right hand. The left hand remained free to press the left and right arrow keys on an 80 cm-high table placed in front of them. To ensure stability during contractions, a strap was used to secure the right forearm to the armrest, maintaining a consistent position.

Task

We employed a well-established EBDM task[6,11,13]. The task was developed using custom-made Matlab code, implemented with the Psychtoolbox library[108]. During this task, participants had to decide whether or not to exert varying levels of physical effort to earn different amounts of monetary rewards. The effort required an isometric contraction of the right biceps. Participants were instructed to attempt bringing their fist closer to their shoulder while keeping their elbow on the armrest and gripping the fixed handle. Real-time electromyography (EMG) was used to measure the strength of the contraction. Monetary rewards were provided in euro cents, and participants were informed that all the money they earned during the task would be theirs to keep.

Each trial began with the presentation of a vertical gauge and a black horizontal line within it, indicating the amount of force the subject needed to exert. Next to the gauge, the amount of money at stake was displayed (Figure 1.B). The gauge size represented 100 % of the maximal voluntary contraction (MVC), determined before the blocks of trials (see *Blocks of trials and MVC* for details). Within each trial, participants were required to exert 20, 40, 60, or 80 % of the MVC, to earn rewards of 1, 5, 10, or 20 cents, leading to 16 possible effort/reward conditions. They had 5 seconds to decide whether to engage in the contraction or not, using the right or left arrow keys on the keyboard positioned under their left hand (*i.e.*, to accept or refuse the contraction, respectively).

If they accepted the trial, a "Go" signal appeared on the screen 1 to 1.2 seconds after making their choice, indicating the start of the contraction period. Participants were provided with continuous biofeedback of their contraction level (see Fig. X), visually represented by the gauge filling. The filling of the gauge was determined by the rectified amplitude of the EMG signal recorded from the right biceps. The participants were required to maintain the contraction at least equal to the level required (*i.e.*, 20, 40, 60 or 80 % of MVC) for a minimum of 2.7 seconds during a 4-second duration (*i.e.*, 2.7 seconds > 66 % of 4 seconds). At the end of each trial, a visuo-auditory feedback was provided to inform participants about the success or failure of their attempt and whether they earned the reward at stake. Trials where muscular contraction was detected before the "Go" signal were directly interrupted, and a "Anticipated" message appeared on the screen. The next trial began 2 seconds later, allowing participants time to recover.

If they refused the trial, the trial ended, and a blank screen appeared before the next trial started 2 seconds later. Additionally, if no decision was made during the initial 5-second period, the trial ended, and the next one began.

Blocks of trials and MVC

Subjects first performed an MVC, allowing us to calibrate the force level required during the EBDM task. During the MVC assessment, we verbally encouraged them to flex their arm as strong as possible during 5 s for three consecutive repetitions with a 30 s rest in-between. The MVC was considered as being the maximal contraction achieved during one of the three repetitions, with the mean between the second and fourth second being taken as the result for each repetition.

Participants then performed a practice block of 16 trials, so that they could get used to the task and have an idea of the force required to reach the different percentages of their MVC. Once the familiarization completed, they performed 5 blocks of 32 trials, each block including two repetitions of each of the 16 effort/reward conditions. There were therefore 160 trials in total, with 10 trials per condition. Conditions were presented in a randomized manner within each block.

A new MVC was measured 30 s after the end of each block. A rest period of 90 s was given to the subject following the MVC acquisition, after which the next block was realized. Hence, the MVC was assessed 6 times during the experiment: before each of the 5 blocks and after the last one. We exploited the MVC so that the required force during each block was readjusted with regards to the putative fatigue in each subject. Importantly, subjects were not aware that the required force during the blocks was readjusted based on the last MVC recorded.

Questionnaires

In the final part of session 2, participants completed three questionnaires on a computer, implemented using the Psytoolkit software. These questionnaires aimed to

measure inter-individual differences in three key variables of interest for our study: apathy, depression and anhedonia, as detailed below.

Apathy

We utilized the extended version of the Lille Apathy Rating Scale (LARS-e), adapted for a healthy population by Bonnelle et al. (2015). The LARS-e consists of 51 items, with 5 propositions for each item, and grades ranging from 1 to 5 for each item, reflecting the subject's level of motivation (a higher number indicating higher motivation). The apathy score is calculated by subtracting the score of each item from the maximum score of 5, then summing up the corresponding items. The obtained sum is divided by the number of items taken, resulting in a mean score between 1 and 5, with a higher score indicating a higher level of apathy[18] (see *Data processing* section below).

Depression

Given that apathy is highly prevalent in depression[13] and that depression is associated with changes in MEP amplitudes[109], it was crucial to assess the level of depression to control for potential confounding factors when examining the relationship between MEP amplitudes and apathy scores. For this purpose, we utilized the Depression Anxiety Stress Scales (DASS 21; as in [18]), a self-report questionnaire comprising 3 subscales: depression, anxiety, and stress. Each subscale contains 7 items, and each item has 4 propositions, with scores ranging from 0 to 3. The total score for each subscale is obtained by summing up the corresponding items.

Anhedonia

Anhedonia is defined as the loss of the ability to experience interest or pleasure in activities that were previously enjoyed. While apathy and anhedonia are two distinct but closely related syndromes, both associated with amotivation, some studies have

shown a positive correlation between these two syndromes in certain conditions such as Parkinson's disease and schizophrenia[13]. Thus, it was essential to ensure that any relationship between MEP amplitudes and apathy scores was specific to apathy and did not concern anhedonia. To measure anhedonia, we used the French version of the Snaith-Hamilton Pleasure Scale (SHAPS)[110]. The SHAPS consists of 14 items, and each item is assigned either 0 or 1 point. The total score ranges from 0 to 14, reflecting the level of anhedonia.

Data processing

Questionnaires data processing

The responses of all participants to each item of the questionnaire were recorded and stored in the Psytoolkit software, and later exported to R (R Core Team, 2020) for further analysis. We calculated the total score for both the LARS-e and the SHAPS. Regarding the DASS-21, we computed only the score for each subscale (depression, anxiety, and stress) since the objective of this scale is not to provide a summation of all the items. We focused on the depression score in the statistical analyses. The distribution of apathy scores is provided in Figure 1.A, while distributions of anhedonia and depression scores are provided in Supplementary Figure 1.

Computation phenotyping of decision-making

We perform computational phenotyping of individuals' behavior in an effort-based decision-making task to estimate inter-individual differences in effort and reward valuation. Our model yielded us an estimation of how these variables influenced the value of an offer for each participant. Based on previous literature[8,10,111], we tested candidate models of value computation, using standard methods (minimization of Bayesian information criterion (BIC) and visual inspection of model fits, see Supplementary Figure 2). More specifically, for each trial, the model computes a subjective value of the offer that depends on the proposed effort and reward. This value is then transformed to an estimated probability of acceptance (between 0 and

1) based on a softmax function[8]. Parameter estimates were determined with the function fmincon on Matlab 2022b (Matlab, Mathworks, USA) with the goal to minimize the difference between each participant's modelled and real choice data (*i.e.*, to minimize the negative log-likelihood of the model given the data). The winning model was the following:

$$Value = \beta_{Effort} \times EFFORT_{LEVEL}.^2 \times (1 + \beta_{Time} \times t) + \beta_{Reward} \times REWARD_{LEVEL} + \beta_0$$

Here, the value of an offer depends on a quadratic function of the proposed $EFFORT_{LEVEL}$ and on the available $REWARD_{LEVEL}$ (modulated by the β_{Effort} and β_{Reward} parameters, respectively). To account for potential time-on-task effects on value computation (due to the repetition of trials), this model also includes a β_{Time} parameter that linearly modulated the cost term based on the trial number[10]. β_0 represents the baseline tendency to accept an offer (the value of accepting an offer for 0 reward). Following model fitting, we obtained for each subject β_{Effort} and β_{Reward} parameters, which we took as proxy of effort and reward valuation, respectively. As such, in the above equation, the more negative the β_{Effort} is, the stronger effort valuation iss (*i.e.*, the stronger the decrease of acceptance rates as a function increasing effort levels). Conversely, the more positive β_{Reward} was, the stronger reward valuation was (*i.e.*, the stronger the increase of acceptance rates as a function increasing reward levels). Also, to facilitate interpretation of the correlations, β_{Effort} values were multiplied by -1 before proceeding with statistical analyses, such that positive β_{Effort} values reflected stronger effort valuation.

Streamline tractography analysis

We utilized the multi-shell, multi-tissue constrained spherical deconvolution (MSMT-CSD) algorithm[112] for local modeling. Streamlines were obtained using the iFOD2 tractography algorithm from MRTrix3 (v3.0.3)[113] with the following parameters: 100,000 streamlines, a maximum angle of 15°, a step size of 1 mm, and a cutoff value of 0.1. The tractograms were then filtered down to 50,000 streamlines using the SIFT algorithm to improve the fit between the density of the streamlines generated and the diffusion signal[48].

For structural connectivity analysis, we used the human Brainnetome atlas [Fan et al., 2016]. The registration of the atlas was conducted using a two-step process: first, a rigid registration aligned the diffusion-weighted MRI data to the T1-weighted MRI subject space. Next, a non-rigid transformation was applied to align the T1-weighted subject space with the MNI template space. This procedure utilized a Python implementation of the ANTS algorithm [Avants et al., 2008]. The transformations obtained were used to register the atlas ROIs to the subject diffusion MRI space, followed by a 2 mm dilation of the ROIs to include the white-gray matter interface. Connectivity matrices were constructed from the filtered tractograms, representing all connections between each pair of structures in the atlas. Brain structures were considered connected if any part of a streamline passed through both ROIs. Given that the number of streamlines is an estimation that can fluctuate from one iteration to another, we run the full analysis for 50 iterations, resulting in 50 connectivity matrices per subject. We then calculated the average number of streamlines for each pair of structures out of the 50 iterations to obtain an average connectivity matrix for each subject. This approach allowed us to obtain a number of streamlines that was not specific to a given iteration. A higher number of streamlines between two structures in the connectivity matrix (*i.e.*, after correction by SIFT) in one subject compared to another, reflects a greater probability that the fibers linking these two regions are more numerous, occupy a larger volume, or are in better condition, thus indicating greater structural connectivity.

As for our TMS data, we focused on the left hemisphere and selected pairs of structures from the matrices that comprised the fronto-BG-M1 and fronto-M1 circuits of interest in the present study. Specifically, we examined the following structures: the SMA, the OFC, the M1, and all structures of the BG that were identifiable using the Brainnetome atlas. These included the dorsal Caudate (dCaudate), the ventral Caudate (vCaudate), the dorsolateral Putamen (dlPutamen), the ventromedial Putamen (vmPutamen), and the Nucleus Accumbens (NAcc). To ensure the completeness of the circuits, we also incorporated the motor part of the thalamus. We extracted the number of streamlines for the following 19 pairs of structures: SMA-M1, SMA-dCaudate, SMA-vCaudate, SMA-dlPutamen, SMA-vmPutamen, SMA-NAcc, OFC-M1, OFC-dCaudate, OFC-vCaudate, OFC-dlPutamen, OFC-vmPutamen, OFC-NAcc, dCaudate-GP, vCaudate-GP, dlPutamen-GP, vmPutamen-GP, NAcc-GP, GP-

Thalamus, and Thalamus-M1. Our objective was to determine whether any of these pairs exhibited an association in terms of structural connectivity (*i.e.*, of number of streamlines) with apathy scores, β_{Effort}, and β_{Reward}.

TMS data processing

The EMG data were analyzed using custom Signal and R scripts (R Core Team, 2020). We applied the same data processing procedure on MEPs obtained in dual-coil and in single-coil ppTMS blocks. First, trials in which the root mean square of the EMG signal exceeded 200 µV before stimulation (*i.e.*, -250 to -50 ms from the pulse) were excluded from the analysis. Second, MEPs with an amplitude exceeding 3 SD around the mean within a given condition were also discarded to reduce MEP variability effects. After applying this cleaning procedure, we retained an average of 22 trials for each condition. The minimum and maximum numbers of MEPs per condition was 17 and 24, respectively. Third, we computed the mean peak-to-peak MEP amplitude for each subject and condition. Finally, we computed a ratio expressing MEP amplitudes elicited by the TS in paired-pulse trials relative to MEP amplitudes elicited by the TS in single-pulse trials. This procedure yielded one MEP ratio for each subject and condition (i.e., for short and long-latency SMA and OFC circuits in dual-coil blocks and for GABAa, GABAb and glutamatergic circuits in single-coil blocks). Ratios above 1 were considered indicative of a facilitatory influence of the CS on MEP amplitude, while ratios below 1 were interpreted as reflecting a suppressive effect. Our objective was to determine whether any of these measures of effective connectivity exhibited an association with apathy scores, β_{Effort}, and β_{Reward}.

Statistical analyses

All statistical analyses were performed using custom-made R scripts (R Core Team, 2020). Our goal was to determine which independent variables quantifying structural connectivity (*i.e.*, the average numbers of streamlines in the tracts of interest) and effective connectivity (*i.e.*, MEP ratios) would be associated with our three dependent variables of interest: apathy scores, β_{Effort} and β_{Reward}. To address this issue, we exploited a conservative two-step statistical approach.

Step 1: independent variable selection with LASSO regression

First, we utilized Least Absolute Shrinkage and Selection Operator (LASSO) regression to perform independent variable selection. LASSO shrinks some regression coefficients to zero, thus eliminating less relevant independent variables.

The LASSO regression can be described by the following equation:

$$\hat{\beta} = \underset{\beta}{\operatorname{argmin}} \left\{ \frac{1}{2n} \sum_{i=1}^{n} (y_i - x_i^T \beta)^2 + \lambda \sum_{j=1}^{p} |\beta_j| \right\}$$

Where y_i represents the response variable for the *i*-th observation, x_i is the vector of independent variables for the *i*-th observation, $\boldsymbol{\beta}$ is the vector of regression coefficients, *n* is the number of observations, *p* is the number of predictors, λ is the regularization parameter controlling the shrinkage of the regression coefficients associated with each independent variable.

The first term, $\frac{1}{2n}\sum_{i=1}^{n}(y_i - x_i^T \beta)^2$, represents the residual sum of squares, which measures the fit of the model (*i.e.*, as in classical regression model, without regularization term). The second term, $\lambda \sum_{j=1}^{p} |\beta_j|$ is the regularization term, which penalizes the absolute values of the coefficients β_j, shrinking less important regression coefficients towards zero as λ increases.

To estimate the optimal value of the regularization parameter λ, a 10-fold cross-validation is classically exploited in the following manner: 1. Partitioning the data: the dataset was randomly split into 10 equal-sized subsets (folds). 2. Training and validation: for each fold, the model was trained on 9 folds (training set) and tested on the remaining fold (validation set). This process was repeated 10 times, each time using a different fold for validation. 3. Model evaluation: for each iteration, the mean squared error (MSE) was calculated to measure the model's predictive accuracy. 4. Averaging the errors: the MSE was averaged across all folds to compute the overall cross-validated error for each λ value. 5. Optimal λ selection: the λ value that minimized the average cross-validated MSE was selected as the optimal parameter. Finally, given that the λ parameter is an estimation that can fluctuate from one iteration

to another, we run the cross-validation for each of the six LASSO regressions for 100 iterations and calculated the average λ parameter out of the 100 iterations.

Once the average optimal λ value was determined (the one that minimizes MSE), the LASSO regression is classically refit on the dataset using this λ value. During this final fitting step, the LASSO algorithm thus selects the β coefficients that balance the trade-off between minimizing MSE and penalizing larger β coefficients. Some β values will be shrunk to zero, meaning the corresponding independent variables are excluded from the regression model. Non-zero β values correspond to the most important independent variables that contribute to explaining the dependent variable (*i.e.*, apathy scores, β_{Effort}, and β_{Reward} in the present study).

Step 2: Partial correlations controlling for potentially confounding variables

Once relevant independent variables selected by the LASSO regression, we performed partial correlations between the dependent variables and the selected independent variables. This was done to control for multiple potentially confounding variables that may covary with apathy, ensuring that the associations we draw between structural or effective connectivity and apathy are specific to apathy. The control variables in our study included age, gender, depression score, and anhedonia score. The partial correlation provided an R-value and a p-value for each correlation. We set the significance level at $p < .05$.

REFERENCES

1. Costello, H., Husain, M. & Roiser, J. P. Apathy and Motivation: Biological Basis and Drug Treatment. *Annu Rev Pharmacol Toxicol* **64**, undefined-undefined (2024).

2. Gilmour, W. *et al.* Impaired value-based decision-making in Parkinson's disease apathy. *Brain* (2024) doi:10.1093/BRAIN/AWAE025.

3. Salamone, J. D. & Correa, M. The Neurobiology of Activational Aspects of Motivation: Exertion of Effort, Effort-Based Decision Making, and the Role of Dopamine. *Annu Rev Psychol* **75**, 1–32 (2024).

4. Kaliuzhna, M. *et al.* Adaptive coding of reward in schizophrenia, its change over time and relationship to apathy. *Brain* **147**, 2459–2470 (2024).

5. Atkins, K. J., Andrews, S. C., Stout, J. C. & Chong, T. T. J. The effect of Huntington's disease on cognitive and physical motivation. *Brain* **147**, 2449–2458 (2024).

6. Morris, L.-A. *et al.* Decision cost hypersensitivity underlies Huntington's disease apathy. *Brain* **139**, 16–17 (2012).

7. Le Heron, C. *et al.* Distinct effects of apathy and dopamine on effort-based decision-making in Parkinson's disease. *Brain* **141**, 1455–1469 (2018).

8. Le Heron, C. *et al.* Dysfunctional effort-based decision-making underlies apathy in genetic cerebral small vessel disease. *Brain* **141**, 3193–3210 (2018).

9. Saleh, Y. *et al.* Apathy in small vessel cerebrovascular disease is associated with deficits in effort-based decision making. *Brain* **144**, 1247–1262 (2021).

10. Pessiglione, M., Vinckier, F., Bouret, S., Daunizeau, J. & Le Bouc, R. Why not try harder? Computational approach to motivation deficits in neuro-psychiatric diseases. *Brain* **141**, 629–650 (2018).

11. Le Bouc, R. *et al.* Effort avoidance as a core mechanism of apathy in frontotemporal dementia. *Brain* **146**, 712–726 (2023).

12. Le Heron, C., Holroyd, C. B., Salamone, J. & Husain, M. Brain mechanisms underlying apathy. *J Neurol Neurosurg Psychiatry* **90**, 302–312 (2019).

13. Husain, M. & Roiser, J. P. Neuroscience of apathy and anhedonia: A transdiagnostic approach. *Nat Rev Neurosci* **19**, 470–484 (2018).

14. Costello, H., Husain, M. & Roiser, J. P. Apathy and Motivation: Biological Basis and Drug Treatment. *Annu Rev Pharmacol Toxicol* **64**, 313–338 (2024).

15. Makin, T. R. & De Xivry, J. J. O. Ten common statistical mistakes to watch out for when writing or reviewing a manuscript. *Elife* **8**, (2019).

16. Ang, Y. S., Lockwood, P., Apps, M. A. J., Muhammed, K. & Husain, M. Distinct Subtypes of Apathy Revealed by the Apathy Motivation Index. *PLoS One* **12**, e0169938 (2017).

17. Spalletta, G., Fagioli, S., Caltagirone, C. & Piras, F. Brain microstructure of subclinical apathy phenomenology in healthy individuals. *Hum Brain Mapp* **34**, 3193–3203 (2013).

18. Bonnelle, V., Manohar, S., Behrens, T. & Husain, M. Individual Differences in Premotor Brain Systems Underlie Behavioral Apathy. *Cerebral Cortex* **26**, 807–819 (2016).

19. Bonnelle, V. *et al.* Characterization of reward and effort mechanisms in apathy. *J Physiol Paris* **109**, 16–26 (2015).

20. Lafond-Brina, G., Pham, B. T. & Bonnefond, A. Specific mechanisms underlying executive and emotional apathy: A phenotyping study. *J Psychiatr Res* **172**, 35–46 (2024).

21. Giulia, L. B. & Anne, B. The stability of multidimensional subclinical apathy during a pandemic and its relations to psycho-behavioral factors. *Sci Rep* **12**, (2022).

22. Kroemer, N. B., Burrasch, C. & Hellrung, L. *To Work or Not to Work: Neural Representation of Cost and Benefit of Instrumental Action*. *Progress in Brain Research* vol. 229 (Elsevier B.V., 2016).

23. Heron, L. Brain mechanisms underlying apathy. *J Neurol Neurosurg Psychiatry* **90**, 302–312 (2019).

24. Alexopoulos, G. S. *et al.* Functional connectivity in apathy of late-life depression: a preliminary study. *J Affect Disord* **149**, 398–405 (2013).

25. Baggio, H. C. *et al.* Resting-state frontostriatal functional connectivity in Parkinson's disease-related apathy. *Mov Disord* **30**, 671–679 (2015).

26. Tay, J. *et al.* Apathy is associated with large-scale white matter network disruption in small vessel disease. *Neurology* **92**, E1157–E1167 (2019).

27. Croxson, P. L., Walton, M. E., O'Reilly, J. X., Behrens, T. E. J. & Rushworth, M. F. S. Effort-based Cost-benefit valuation and the human brain. *Journal of Neuroscience* **29**, 4531–4541 (2009).

28. Zénon, A., Sidibé, M. & Olivier, E. Disrupting the supplementary motor area makes physical effort appear less effortful. *Journal of Neuroscience* **35**, 8737–8744 (2015).

29. Huang, C. *et al.* Neuroimaging markers of motor and nonmotor features of Parkinson's disease: an 18f fluorodeoxyglucose positron emission computed tomography study. *Dement Geriatr Cogn Disord* **35**, 183–196 (2013).

30. Stoll, F. M. & Rudebeck, P. H. Preferences reveal dissociable encoding across prefrontal-limbic circuits. *Neuron* **112**, 2241-2256.e8 (2024).

31. Hogan, P. S., Galaro, J. K. & Chib, V. S. Roles of Ventromedial Prefrontal Cortex and Anterior Cingulate in Subjective Valuation of Prospective Effort. *Cerebral Cortex* **29**, 4277–4290 (2019).

32. Carriere, N. *et al.* Apathy in Parkinson's disease is associated with nucleus accumbens atrophy: a magnetic resonance imaging shape analysis. *Mov Disord* **29**, 897–903 (2014).

33. Robert, G. H. *et al.* Preoperative factors of apathy in subthalamic stimulated Parkinson disease: a PET study. *Neurology* **83**, 1620–1626 (2014).

34. Suzuki, S., Lawlor, V. M., Cooper, J. A., Arulpragasam, A. R. & Treadway, M. T. Distinct regions of the striatum underlying effort, movement initiation and effort discounting. *Nat Hum Behav* (2020) doi:10.1038/s41562-020-00972-y.

35. Hollunder, B. *et al.* Mapping dysfunctional circuits in the frontal cortex using deep brain stimulation. *Nature Neuroscience 2024 27:3* **27**, 573–586 (2024).

36. Cisek, P. & Kalaska, J. F. Neural Mechanisms for Interacting with a World Full of Action Choices. *Annu Rev Neurosci* **33**, 269–298 (2010).

37. Cisek, P. & Pastor-Bernier, A. On the challenges and mechanisms of embodied decisions. *Philosophical Transactions of the Royal Society B: Biological Sciences* **369**, 20130479–20130479 (2014).

38. Derosiere, G. & Duque, J. Tuning the Corticospinal System: How Distributed Brain Circuits Shape Human Actions. *Neuroscientist* Preprint at https://doi.org/10.1177/1073858419896751 (2020).

39. Levy, S. *et al.* Cell-Type-Specific Outcome Representation in the Primary Motor Cortex. *Neuron* **107**, 954-971.e9 (2020).

40. Lee, C., Harkin, E. F., Yin, X., Naud, R. & Chen, S. Cell-type-specific responses to associative learning in the primary motor cortex. *Elife* **11**, (2022).

41. Ramakrishnana, A. *et al.* Cortical neurons multiplex reward-related signals along with sensory and motor information. *Proc Natl Acad Sci U S A* **114**, E4841–E4850 (2017).

42. Klein-Flugge, M. C., Bestmann, S., Klein-Flügge, M. C. & Bestmann, S. Time-Dependent Changes in Human Corticospinal Excitability Reveal Value-Based Competition for Action during Decision Processing. *Journal of Neuroscience* **32**, 8373–8382 (2012).

43. Klein, P. A., Olivier, E. & Duque, J. Influence of reward on corticospinal excitability during movement preparation. *Journal of Neuroscience* **32**, 18124–18136 (2012).

44. Cos, I., Duque, J. & Cisek, P. Rapid prediction of biomechanical costs during action decisions. *J Neurophysiol* **112**, 1256–1266 (2014).

45. Derosiere, G., Zénon, A., Alamia, A. & Duque, J. Primary motor cortex contributes to the implementation of implicit value-based rules during motor decisions. *Neuroimage* **146**, 1115–1127 (2017).

46. Derosiere, G., Vassiliadis, P., Demaret, S., Zénon, A. & Duque, J. Learning stage-dependent effect of M1 disruption on value-based motor decisions. *Neuroimage* **162**, 173–185 (2017).

47. Harris, A. & Lim, S. L. Temporal dynamics of sensorimotor networks in effort-based cost-benefit valuation: Early emergence and late net value integration. *Journal of Neuroscience* **36**, 7167–7183 (2016).

48. Smith, R. E., Tournier, J. D., Calamante, F. & Connelly, A. SIFT2: Enabling dense quantitative assessment of brain white matter connectivity using streamlines tractography. *Neuroimage* **119**, 338–351 (2015).

49. Yeh, C. H., Smith, R. E., Dhollander, T., Calamante, F. & Connelly, A. Connectomes from streamlines tractography: Assigning streamlines to brain parcellations is not trivial but highly consequential. *Neuroimage* **199**, 160–171 (2019).

50. Di Lazzaro, V., Rothwell, J. & Capogna, M. Noninvasive Stimulation of the Human Brain: Activation of Multiple Cortical Circuits. *Neuroscientist* vol. 24 246–260 Preprint at https://doi.org/10.1177/1073858417717660 (2018).

51. Neige, C. *et al.* Connecting the dots: harnessing dual-site transcranial magnetic stimulation to quantify the causal influence of medial frontal areas on the motor cortex. *Cerebral Cortex* (2023) doi:10.1093/CERCOR/BHAD370.

52. Attaallah, B. *et al.* The role of the human hippocampus in decision-making under uncertainty. *Nature Human Behaviour 2024 8:7* **8**, 1366–1382 (2024).

53. Morris, L.-A. *et al.* Decision cost hypersensitivity underlies Huntington's disease apathy. *Brain* **139**, 16–17 (2012).

54. Chong, T. T. J., Bonnelle, V. & Husain, M. *Quantifying Motivation with Effort-Based Decision-Making Paradigms in Health and Disease*. *Progress in Brain Research* vol. 229 (Elsevier B.V., 2016).

55. Muhammed, K., Dalmaijer, E., Manohar, S. & Husain, M. Voluntary modulation of saccadic peak velocity associated with individual differences in motivation. *Cortex* **122**, 198–212 (2020).

56. Saleh, Y. *et al.* Apathy in small vessel cerebrovascular disease is associated with deficits in effort-based decision making. *Brain* **144**, 1247–1262 (2021).

57. Neubert, F. X., Mars, R. B., Buch, E. R., Olivier, E. & Rushworth, M. F. S. Cortical and subcortical interactions during action reprogramming and their related white matter pathways. *Proc Natl Acad Sci U S A* **107**, 13240–13245 (2010).

58. Hogeveen, J. *et al.* Ventromedial Prefrontal-Anterior Cingulate Hyperconnectivity and Resilience to Apathy in Traumatic Brain Injury. *J Neurotrauma* **38**, 2264–2274 (2021).

59. Ashton, S. E. *et al.* Distinct Action Signals by Subregions in the Nucleus Accumbens during STOP–Change Performance. *Journal of Neuroscience* **44**, (2024).

60. Ottenheimer, D., Richard, J. M. & Janak, P. H. Ventral pallidum encodes relative reward value earlier and more robustly than nucleus accumbens. *Nature Communications 2018 9:1* **9**, 1–14 (2018).

61. Detrick, J. A. *et al.* Motor cortex modulation and reward in children with attention-deficit/hyperactivity disorder. *Brain Commun* **3**, (2021).

62. Hamel, R. *et al.* The intracortical excitability changes underlying the enhancing effects of rewards and punishments on motor performance. *Brain Stimul* **16**, 1462–1475 (2023).

63. Bartra, O., McGuire, J. T. & Kable, J. W. The valuation system: A coordinate-based meta-analysis of BOLD fMRI experiments examining neural correlates of subjective value. *Neuroimage* **76**, 412 (2013).

64. Grool, A. M. *et al.* Structural MRI correlates of apathy symptoms in older persons without dementia: AGES-Reykjavik Study. *Neurology* **82**, 1628 (2014).

65. Stanton, B. R., Leigh, P. N., Howard, R. J., Barker, G. J. & Brown, R. G. Behavioural and emotional symptoms of apathy are associated with distinct patterns of brain atrophy in neurodegenerative disorders. *J Neurol* **260**, 2481–2490 (2013).

66. Tunnard, C. *et al.* Apathy and cortical atrophy in Alzheimer's disease. *Int J Geriatr Psychiatry* **26**, 741–748 (2011).

67. Klaasen, N. G., Kos, C., Aleman, A. & Opmeer, E. M. Apathy is related to reduced activation in cognitive control regions during set-shifting. *Hum Brain Mapp* **38**, 2722–2733 (2017).

68. Holthoff, V. A. *et al.* Regional cerebral metabolism in early Alzheimer's disease with clinically significant apathy or depression. *Biol Psychiatry* **57**, 412–421 (2005).

69. Kawagoe, T., Onoda, K. & Yamaguchi, S. Apathy and executive function in healthy elderly-resting state fMRI study. *Front Aging Neurosci* **9**, 263893 (2017).

70. Siegel, J. S. *et al.* The circuitry of abulia: insights from functional connectivity MRI. *Neuroimage Clin* **6**, 320–326 (2014).

71. Whitfield-Gabrieli, S. *et al.* Hyperactivity and hyperconnectivity of the default network in schizophrenia and in first-degree relatives of persons with schizophrenia. *Proc Natl Acad Sci U S A* **106**, 1279–1284 (2009).

72. Lynch, C. J. *et al.* Frontostriatal salience network expansion in individuals in depression. *Nature 2024 633:8030* **633**, 624–633 (2024).

73. Oestreich, L. K. L., Wright, P. & O'sullivan, M. J. Hyperconnectivity and altered interactions of a nucleus accumbens network in post-stroke depression. *Brain Commun* **4**, (2022).

74. Leaver, A. M. *et al.* Desynchronization and Plasticity of Striato-frontal Connectivity in Major Depressive Disorder. *Cereb Cortex* **26**, 4337–4346 (2016).

75. Kaiser, R. H., Andrews-Hanna, J. R., Wager, T. D. & Pizzagalli, D. A. Large-Scale Network Dysfunction in Major Depressive Disorder: A Meta-analysis of Resting-State Functional Connectivity. *JAMA Psychiatry* **72**, 603–611 (2015).

76. Brown, P. Abnormal oscillatory synchronisation in the motor system leads to impaired movement. *Curr Opin Neurobiol* **17**, 656–664 (2007).

77. Kondabolu, K. *et al.* Striatal cholinergic interneurons generate beta and gamma oscillations in the corticostriatal circuit and produce motor deficits. *Proc Natl Acad Sci U S A* **113**, 3159–3168 (2016).

78. McCarthy, M. M. *et al.* Striatal origin of the pathologic beta oscillations in Parkinson's disease. *Proc Natl Acad Sci U S A* **108**, 11620–11625 (2011).

79. Li, K. *et al.* Distinguishing between parallel and serial processing in visual attention from neurobiological data. *R Soc Open Sci* **7**, (2020).

80. Lisi, M., Morgan, M. J. & Solomon, J. A. Perceptual decisions and oculomotor responses rely on temporally distinct streams of evidence. *Communications Biology 2022 5:1* **5**, 1–8 (2022).

81. Thura, D., Cabana, J. F., Feghaly, A. & Cisek, P. Integrated neural dynamics of sensorimotor decisions and actions. *PLoS Biol* **20**, e3001861 (2022).

82. Buch, E. R., Johnen, V. M., Nelissen, N., O'Shea, J. & Rushworth, M. F. S. Noninvasive Associative Plasticity Induction in a Corticocortical Pathway of the Human Brain. *Journal of Neuroscience* **31**, 17669–17679 (2011).

83. Turrini, S. *et al.* Cortico-cortical paired associative stimulation (ccPAS) over premotor-motor areas affects local circuitries in the human motor cortex via Hebbian plasticity. *Neuroimage* **271**, 120027 (2023).

84. Kohl, S. *et al.* Cortical Paired Associative Stimulation Influences Response Inhibition: Cortico-cortical and Cortico-subcortical Networks. *Biol Psychiatry* **85**, 355–363 (2019).

85. Bevilacqua, M. *et al.* Single session cross-frequency bifocal tACS modulates visual motion network activity in young healthy population and stroke patients. *Brain Stimul* **17**, 660–667 (2024).

86. Emanuel, A., Herszage, J., Sharon, H., Liberman, N. & Censor, N. Inhibition of the supplementary motor area affects distribution of effort over time. *Cortex* **134**, 134–144 (2021).

87. Kasess, C. H. *et al.* The suppressive influence of SMA on M1 in motor imagery revealed by fMRI and dynamic causal modeling. *Neuroimage* **40**, 828–837 (2008).

88. Johansen-Berg, H. *et al.* Changes in connectivity profiles define functionally distinct regions in human medial frontal cortex. *Proc Natl Acad Sci U S A* **101**, 13335–13340 (2004).

89. Luppino, G., Matelli, M., Camarda, R. & Rizzolatti, G. Corticocortical connections of area F3 (SMA-proper) and area F6 (pre-SMA) in the macaque monkey. *J Comp Neurol* **338**, 114–140 (1993).

90. Muakkassa, K. F. & Strick, P. L. Frontal lobe inputs to primate motor cortex: evidence for four somatotopically organized 'premotor' areas. *Brain Res* **177**, 176–182 (1979).

91. Kupchik, Y. M. & Kalivas, P. W. The Direct and Indirect Pathways of the Nucleus Accumbens are not What You Think. *Neuropsychopharmacology* **42**, 369–370 (2017).

92. Jones, D. L. & Mogenson, G. J. Nucleus accumbens to globus pallidus GABA projection: electrophysiological and iontophoretic investigations. *Brain Res* **188**, 93–105 (1980).

93. Mogenson, G. J., Swanson, L. W. & Wu, M. Neural projections from nucleus accumbens to globus pallidus, substantia innominata, and lateral preoptic-lateral hypothalamic area: an anatomical and electrophysiological investigation in the rat. *J Neurosci* **3**, 189–202 (1983).

94. Bjork, J. M. *et al.* Plasma GABA levels correlate with aggressiveness in relatives of patients with unipolar depressive disorder. *Psychiatry Res* **101**, 131–136 (2001).

95. Dessain, Q., Fuchs, C., Macq, B. & Rensonnet, G. Fast multi-compartment Microstructure Fingerprinting in brain white matter. *Front Neurosci* **18**, (2024).

96. Hoopes, A., Mora, J. S., Dalca, A. V., Fischl, B. & Hoffmann, M. SynthStrip: skull-stripping for any brain image. *Neuroimage* **260**, 119474 (2022).

97. Andersson, J. L. R. & Sotiropoulos, S. N. An integrated approach to correction for off-resonance effects and subject movement in diffusion MR imaging. *Neuroimage* **125**, 1063–1078 (2016).

98. Smith, S. M. *et al.* Advances in functional and structural MR image analysis and implementation as FSL. *Neuroimage* **23 Suppl 1**, (2004).

99. Schilling, K. G. *et al.* Synthesized b0 for diffusion distortion correction (Synb0-DisCo). *Magn Reson Imaging* **64**, 62–70 (2019).

100. Derosiere, G., Vassiliadis, P. & Duque, J. Advanced TMS approaches to probe corticospinal excitability during action preparation. *NeuroImage* vol. 213 116746 Preprint at https://doi.org/10.1016/j.neuroimage.2020.116746 (2020).

101. Wilhelm, E. *et al.* Corticospinal Suppression Underlying Intact Movement Preparation Fades in Parkinson's Disease. *Movement Disorders* **37**, 2396–2406 (2022).

102. Wilhelm, E. *et al.* Subthalamic DBS does not restore deficits in corticospinal suppression during movement preparation in Parkinson's disease. *Clinical Neurophysiology* **165**, 107–116 (2024).

103. Derosiere, G., Thura, D., Cisek, P. & Duque, J. Motor cortex disruption delays motor processes but not deliberation about action choices. *J Neurophysiol* **122**, 1566–1577 (2019).

104. Vassiliadis, P., Derosiere, G., Grandjean, J. & Duque, J. Motor training strengthens corticospinal suppression during movement preparation. *bioRxiv* 2020.02.14.948877 (2020) doi:10.1101/2020.02.14.948877.

105. Yadav, G. *et al.* Effects Of Extrinsic Reward Based Skill Learning On Motor Plasticity. *bioRxiv* 2024.09.10.612238 (2024) doi:10.1101/2024.09.10.612238.

106. Codol, O., Galea, J. M., Jalali, R. & Holland, P. J. Reward-driven enhancements in motor control are robust to TMS manipulation. *Exp Brain Res* **238**, 1781–1793 (2020).

107. Rurak, B. K., Rodrigues, J. P., Power, B. D., Drummond, P. D. & Vallence, A. M. Test Re-test Reliability of Dual-site TMS Measures of SMA-M1 Connectivity Differs Across Inter-stimulus Intervals in Younger and Older Adults. *Neuroscience* **472**, 11–24 (2021).

108. Brainard, D. H. The Psychophysics Toolbox. *Spat Vis* **10**, 433–436 (1997).

109. Lefaucheur, J. P. *et al.* Inter-hemispheric asymmetry of motor corticospinal excitability in major depression studied by transcranial magnetic stimulation. *J Psychiatr Res* **42**, 389–398 (2008).

110. G, L. *et al.* Etude de validation de la version française de l'échelle de plaisir de Snaith et Hamilton (Snaith-Hamilton pleasure scale, SHAPS, Snaith et al. 1995) : détermination des paramètres métrologiques chez 208 sujets sains et chez 103 malades hospitalisés présentant une dépression ou une schizophrénie. *ENCEPHALE* (1997).

111. Prévost, C., Pessiglione, M., Météreau, E., Cléry-Melin, M. L. & Dreher, J. C. Separate valuation subsystems for delay and effort decision costs. *Journal of Neuroscience* **30**, 14080–14090 (2010).

112. Jeurissen, B., Tournier, J. D., Dhollander, T., Connelly, A. & Sijbers, J. Multi-tissue constrained spherical deconvolution for improved analysis of multi-shell diffusion MRI data. *Neuroimage* **103**, 411–426 (2014).

113. Tournier, J. D. Diffusion MRI in the brain - Theory and concepts. *Prog Nucl Magn Reson Spectrosc* **112–113**, 1–16 (2019).